INDC(NDS)-0821
Distr. G+NM+PH

IAEA
International Atomic Energy Agency

INDC International Nuclear Data Committee

Addendum to IAEA(NDS) reports on the neutron capture Photon Strength Functions

Jiri Kopecky
JUKO Research
Alkmaar, The Netherlands

and

Stephane Goriely
Universite Libre de Bruxelles
Belgium

November 2020

IAEA Nuclear Data Section
Vienna International Centre, P.O. Box 100, 1400 Vienna, Austria

Selected INDC documents may be downloaded in electronic form from
http://www-nds.iaea.org/publications
or sent as an e-mail attachment.
Requests for hardcopy or e-mail transmittal should be directed to
NDS.Contact-Point@iaea.org
or to:
Nuclear Data Section
International Atomic Energy Agency
Vienna International Centre
PO Box 100
1400 Vienna
Austria

Printed by the IAEA in Austria

November 2020

INDC(NDS)-0821
Distr. G+NM+PH

Addendum to IAEA(NDS) reports on the neutron capture Photon Strength Functions

Jiri Kopecky
JUKO Research
Alkmaar, The Netherlands

and

Stephane Goriely
Universite Libre de Bruxelles
Belgium

November 2020

Table of Contents

1. Introduction

The Photon Strength Functions (PSF) from the neutron capture have been studied in the frame of the CRP project "*Generating a Reference Database for PSF*" at the NDS in the period 2016 – 2019. The results have been published in six IAEA(NDS) reports and one publication [1-7]. This report briefly summarizes several additional actions: revision and verification of some previous data important for the derivation of the <<f(L)>> systematics, validation of conclusions with new THC f(L) data and their inclusions in the THC data base and few spotted errors corrected. Finally, one section (written by S. Goriely) is devoted to an extended comparison of all these PSF data against the QRSP calculations and comments the results.

The derivation of the <<f (E1, M1)>> systematics has been thoroughly re-addressed, especially the trend outlying data points and their possible influence on the recommended final equations. Several new THC evaluations have been for this purpose processed, especially for the heavier nuclides. This validation resulted that some entries have been corrected or removed and the behavior of the adopted entries are now well understood. The final two systematic equations of <<f(L)>> at $<E_\gamma = 6.5$ MeV> form the best absolute calibration of the E1 and M1 strength functions from the neutron capture.

2. New THC evaluations

After finishing the first THC PSF data base, listed in Ref. [5], several new evaluations have been processed and will be included in the final PSF THC data base. The new evaluations are listed in Table 1. The choice of targets was based on the addition of several targets with A < 70 to make this data base more complete for the study of the presence of nonstatistical components. The addressed heavier mass targets belonged to the PSF data which formed the outliers in the DRC <<f(L)>> analysis (see Chapter 3) and the thermal capture data can be additionally used to verify the validity of the DRC results.

Table 1. Thermal cross section parameters of stable nuclides with new THC measurements after Ref. [7]. Important results are given in columns 3, 4 and 5. They indicate fractions of positive resonance contributions, bound state contributions and the direct capture to the bound state component. No s(D) value reflects no data in Ref. [8]. See Refs. [5,7] for more details.

Target	$\sigma(\gamma)_0$	$\sigma(+) + \sigma(-) = \sigma(res)$	$\sigma(B)$	$\sigma(D)$
	[b]	[b]	[b]	[b]
Ni-58	4.39	0.32	4.07	4.11
Ni-60	2.45	1.44	1.01	1.09
Ni-62	14.9	14.9		9.05
Zn-64	1.11	0.56	0.23	0.155
Zn-67	7.5	3.65	3.85	
Zn-68	1.07	0.97	0.10	0.006
Nb-93	1.15	0.092	1.058	
Ru-99	7.24	7.24	0	
Ru-101	5.2	3.45	1.77	
Yb-173	15.5	8.71	6.79	
Lu-176	2057	2057	0	
W-183	10.4	9.02	1.38	
Th-232	7.35	0.44	6.91	

3. Revision and update of the DRC <f(L)> systematics

The importance of the doubly averaged <<f(E1)>> DRC systematics at the mean gamma ray energy $E_\gamma = (6.5 \pm 0.5)$ MeV [3,4] is that it is the only general absolute normalization for the ARC data, which form the best averaged data set of the E1 and M1 strength behavior. The other possibility is, to use the experimental DRC <f(L)> data directly, however, applicable only if both DRC and ARC data are available for the same nuclide.

A new source of the absolute PSF values has been recently derived using the thermal capture data. The binned f(L) "EGAF" data base has been published by Firestone in Refs. [6,9] for a large number of nuclides, however, the binning takes place at different mean transition energies and smooths away any information on the f(L) energy dependence. But it remains valuable as a single-point information for the processed f(L) data from other experiments.

We have chosen the standard partial processing of the THC data, avoiding any data binning see Refs. [5,7]. It seems, therefore, reasonable to extend and validate the earlier <<f(L>> systematic data using the recent thermal capture data (THC and EGAF data) and to check the <<f(L>> data outliers and their possible influence on the final systematic equation.

3.1 E1 – DRC outliers

The plot of quasi-mono energetic doubly average strength functions <<f(E1)>> from Ref. [3] is used as the basis for the revision (see Fig.1). Data with masses A < 60 are influenced by the presence of the non-statistical effects, which originate from the s, p and d – wave resonances and make the situation rather complex and not discussed as outlying values. However, we do believe that the trend dependence reasonably reflects their mean behavior.

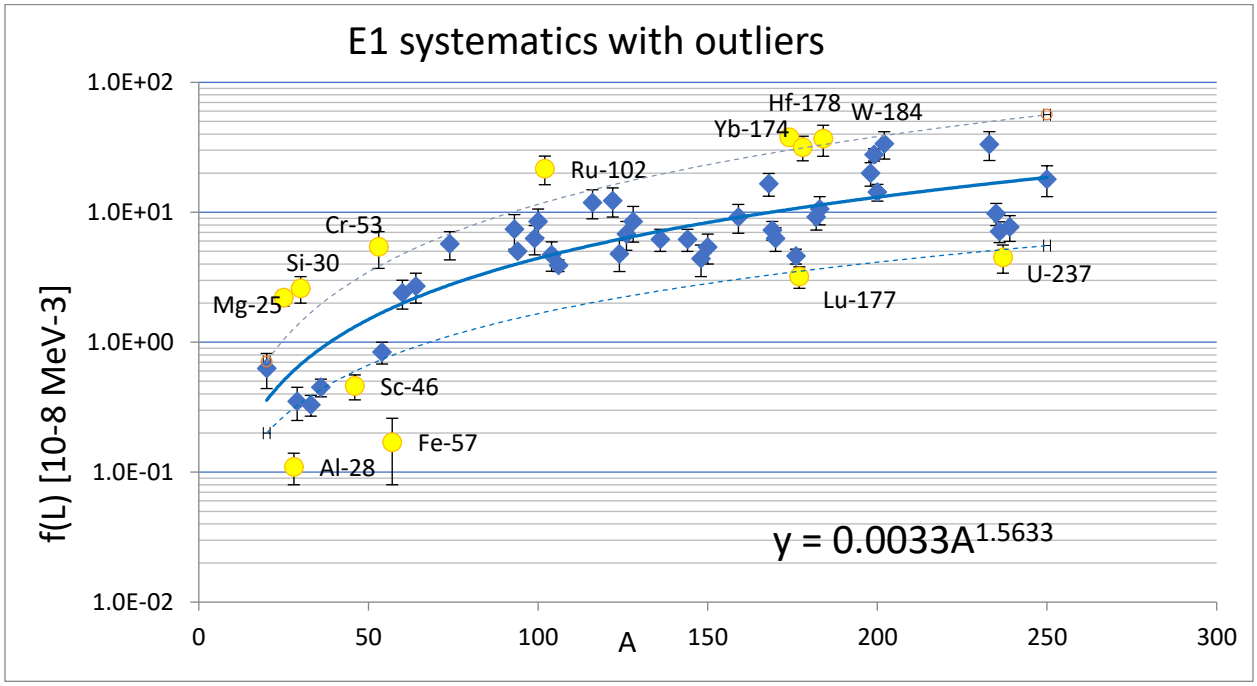

Fig. 2 *Quasi-mono energetic doubly average strength functions <<f(E1)>> from Ref. [3,4] with trend curve systematic as a function of the mass A. The dotted line is one SD dispersion from the assumed LSQ procedure. Data close or outside to dispersion curves have been identified as the outliers (yellow data points).*

Data for masses with A > 70 become statistically significant due to the better averaging from a larger number of s- or p-resonances involved. In such a case any outlying data point may signalize either a normalization uncertainty or indicate a real physical reason for the deviation. The data outliers for masses with A > 70 have been identified as ^{102}Ru, ^{174}Yb, ^{178}Hf, ^{184}W (too large) or ^{177}Lu and ^{237}U (too small). We shall now use the thermal capture data for additional validation of these data.

The difference between the mean energy ($E_\gamma \pm \Delta E_\gamma$) and the systematic E_γ = 6.5 MeV can be a source of additional uncertainty, even if the assumed energy dependence of E_γ^2 is applied. To illustrate the situation the mean E_γ values are plotted in Fig. 3 as a function of A.

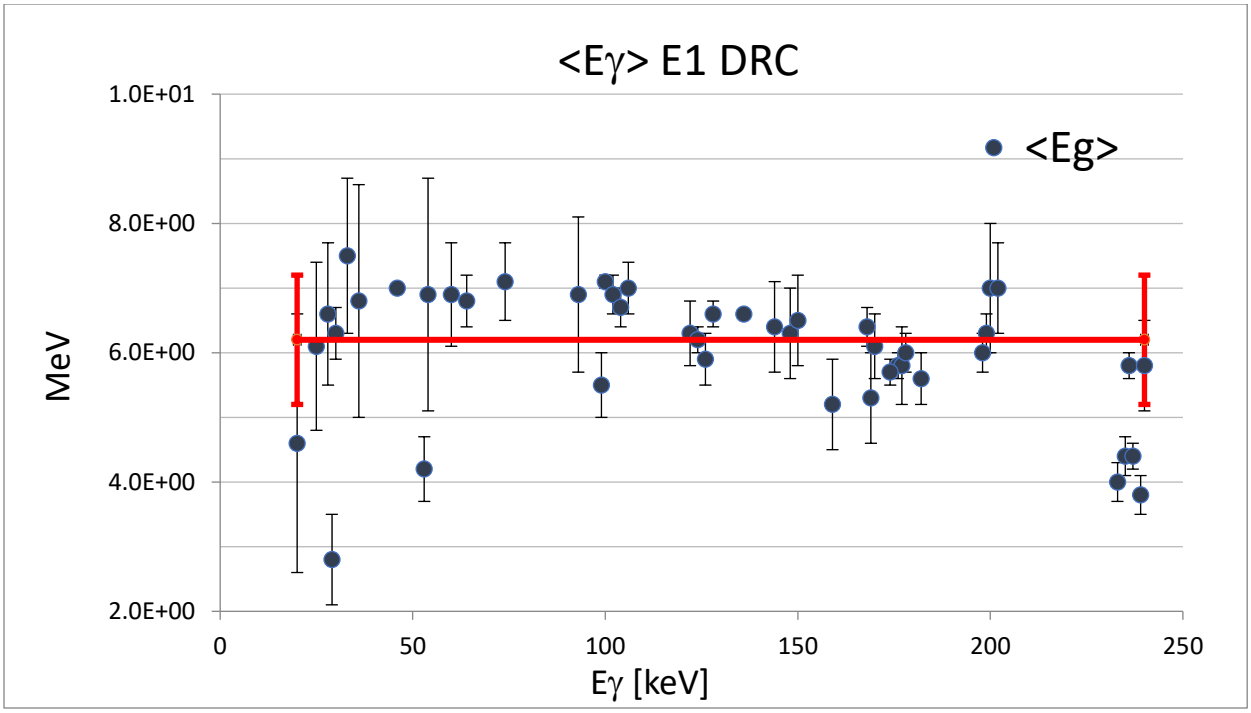

Fig. 3 *The mean energy regions ($E_\gamma \pm \Delta E_\gamma$) of the THC data used to generate the doubly average <<f(L)>> values for the systematic equation. The red curve indicates the mean value of 6.3±1.0 MeV.*

This plot shows that only the actinide targets seriously deviate from the mean $<E_\gamma>$ data and may, if uncorrected, explain some too low <<f(L)>> values. The only strongly deviating data point below A < 50 (^{29}Si) does not seriously influence the trend (due to the presence d-wave non-statistical processes) contrary to the statistical mode of the actinide targets. The PSF outliers are now discussed in detail. Possible sources of the uncertainty or erroneous absolute PSF normalization can be characterized as:

1. Wrong absolute calibration of the measured relative transition probability in either I_γ/neutron capture or $\Gamma_{\gamma i}$ values.
2. Errors in the selection of primary transitions.
3. Errors in transition multipolarity assignments based on the parity of the final states.
4. Uncertainty of the total radiative width $\Gamma_{\gamma o}$
5. Uncertainty of the spacing D and correctness of the l_n and spin J dependence

The important supporting information for the outlying value is if this effect is present for both E1 and M1 multipolarities, sending a signal of the uncertainty in absolute normalization or an erroneous processing of the original experimental data in the PSF values.

Ru-102 – The <<f(L)>> both for E1 and M1 strength are enhanced, which may suggest a common absolute normalization problem. To investigate this situation the new THC Ru-102 data has been processed and together with the binned EGAF data [9] compared in Fig. 4 with DRC data. The comparison shows a rather good agreement and the absolute normalization influence is found minimal and disregarded. This observation is valid both for E1 and M1 radiation. The reason for the enhancement is absent. The <PSF> value confirmed.

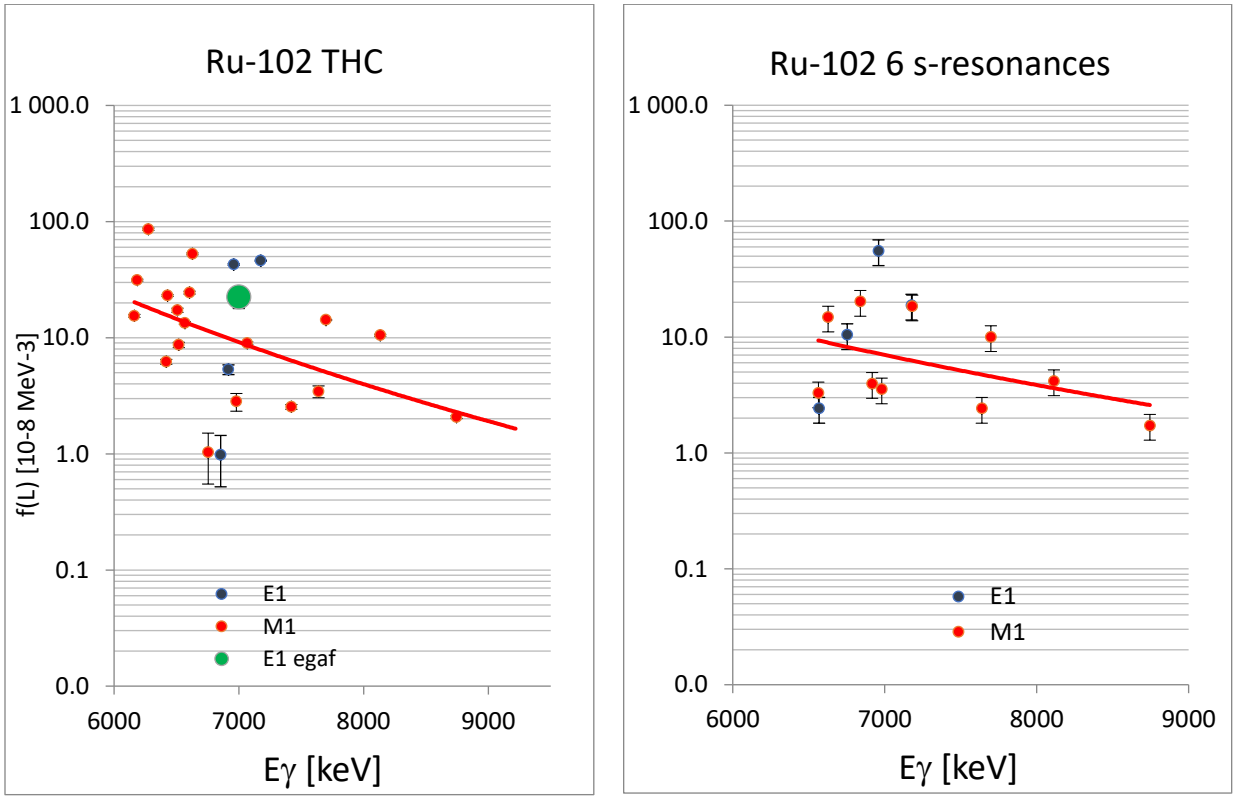

Fig. 4 *Comparison of the THC f(L) 1^{02}Ru data from the recent work and Ref. [9] with the <f(L)> DRC results from Ref. [3]. Note the good agreement between these two independent measurements. The E1 data are in a too narrow energy band and the trend line is not plotted because the shape may be misleading. The green point is the EGAF binned value.*

Yb-174 – The E1 enhancement in both experiments, THC and DRC and the mean trend is in a good agreement. The nucleus was not included in the EGAF data base. The <PSF> value confirmed (see Fig.5).

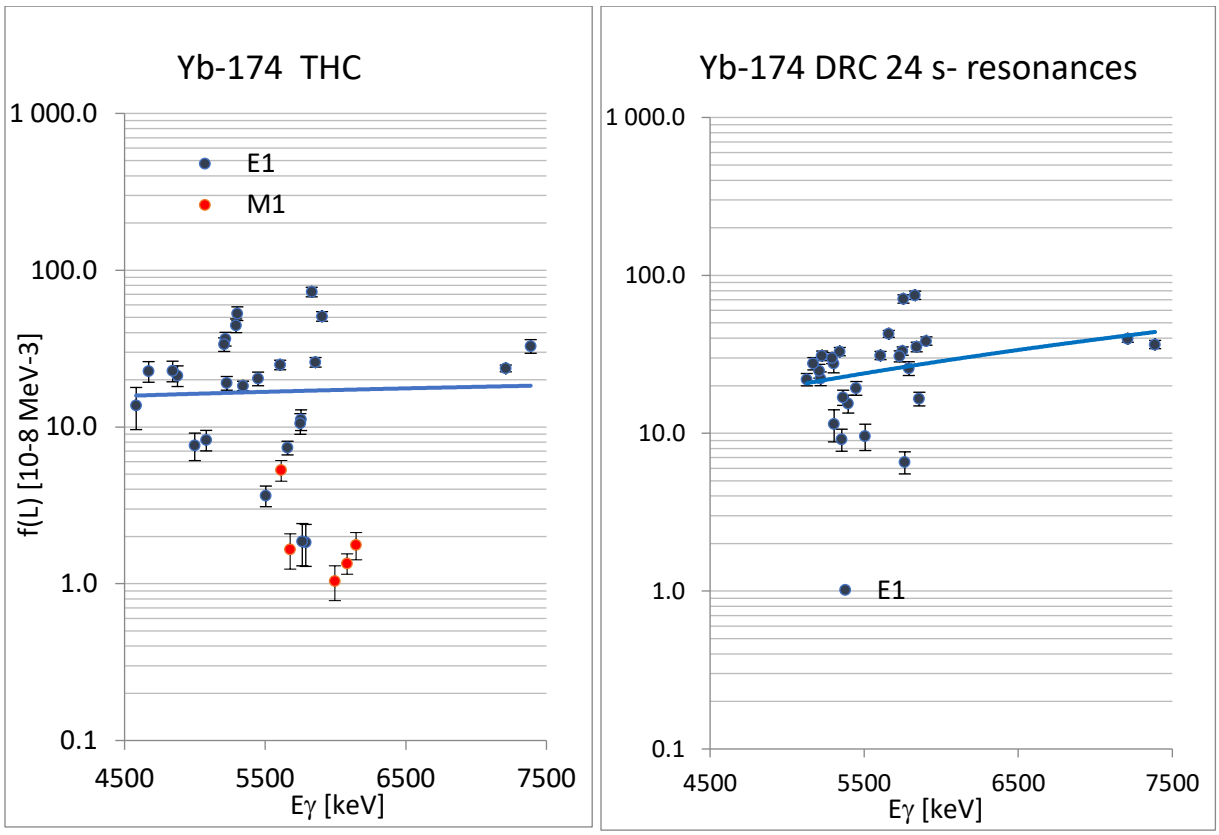

Fig. 5 *Comparison of the THC f(L) ^{174}Yb data from the recent work with the <f(L)> DRC results from Ref. [3]. Note the good agreement between these two independent measurements.*

Hf-178 - The E1 enhancement in both experiments including the independent THC binned data from EGAF, THC and DRC are in a good agreement. The <PSF> value confirmed.

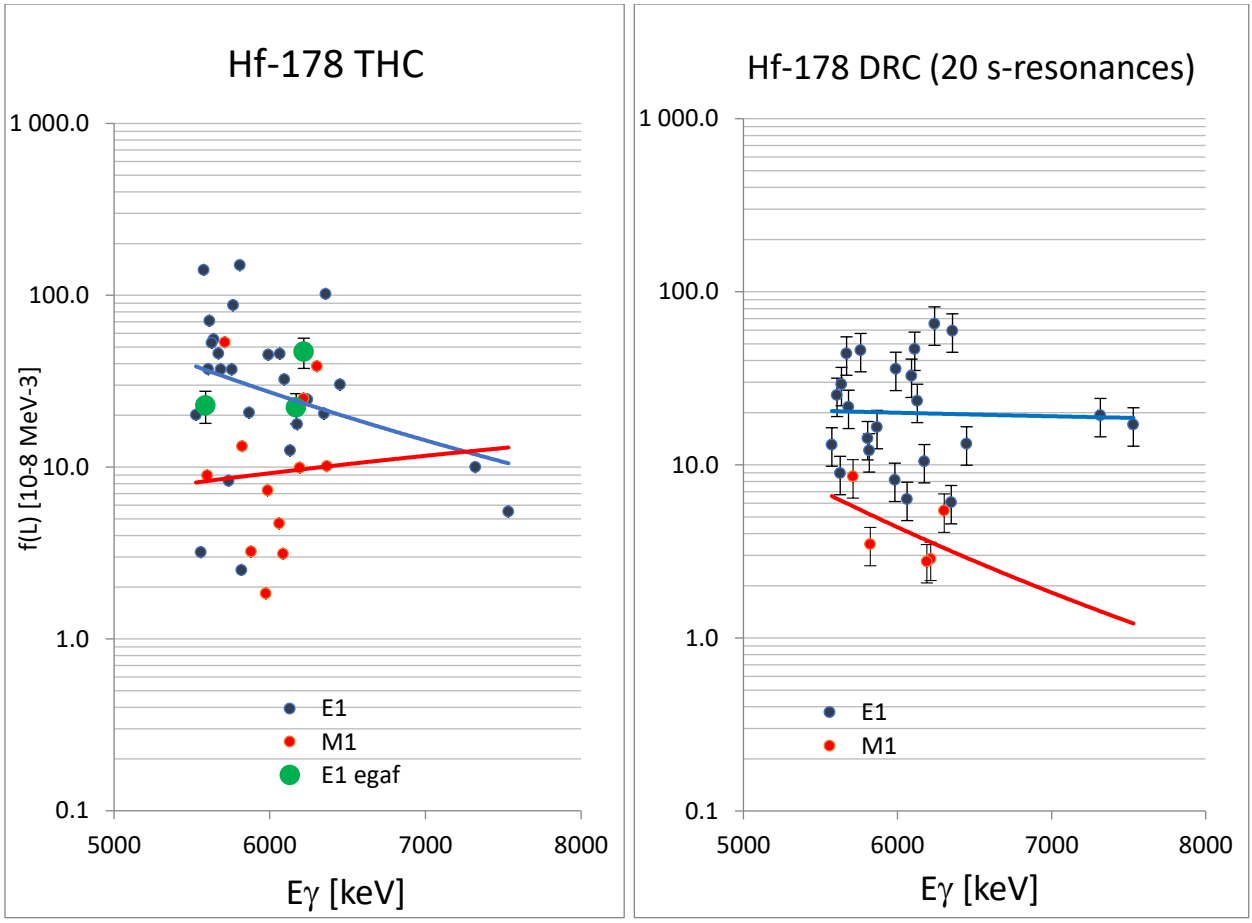

Fig.6 *Comparison of the THC f(L) ^{178}Hf data from the recent work and Ref. [9] with the <f(L)> DRC results from Ref. [3]. Note the good agreement between these two independent measurements. The green points are from the EGAF data base.*

W-184 The situation of the ^{184}W nucleus data is rather complex. Firstly, there is a reasonable agreement between THC partial measurement and the DRC data. In all evaluations the input parameters were similar, D_o = 12 eV or 13.7 eV and $\Gamma_{\gamma o}$ = 0.073 eV. However, the binned TH data from the EGAF library are clearly weaker. For the conversion of the DRC absolute I_γ intensities the width $\Gamma_{\gamma i}$ for each resonance from Ref. [8] have been used. Secondly, the absolute calibration of the THC data is not clear. The transitions intensities are given in relative values, normalization to the absolute intensity I_γ/100 neutrons is based on the application of a normalization factor from an external calibration with limited information about. However, since the DRC data are about equal to the THC data, it means that also in the DRC data the absolute calibration is not correct. No definitive conclusion is available and the <PSF> value remains as an unexplained outlier.

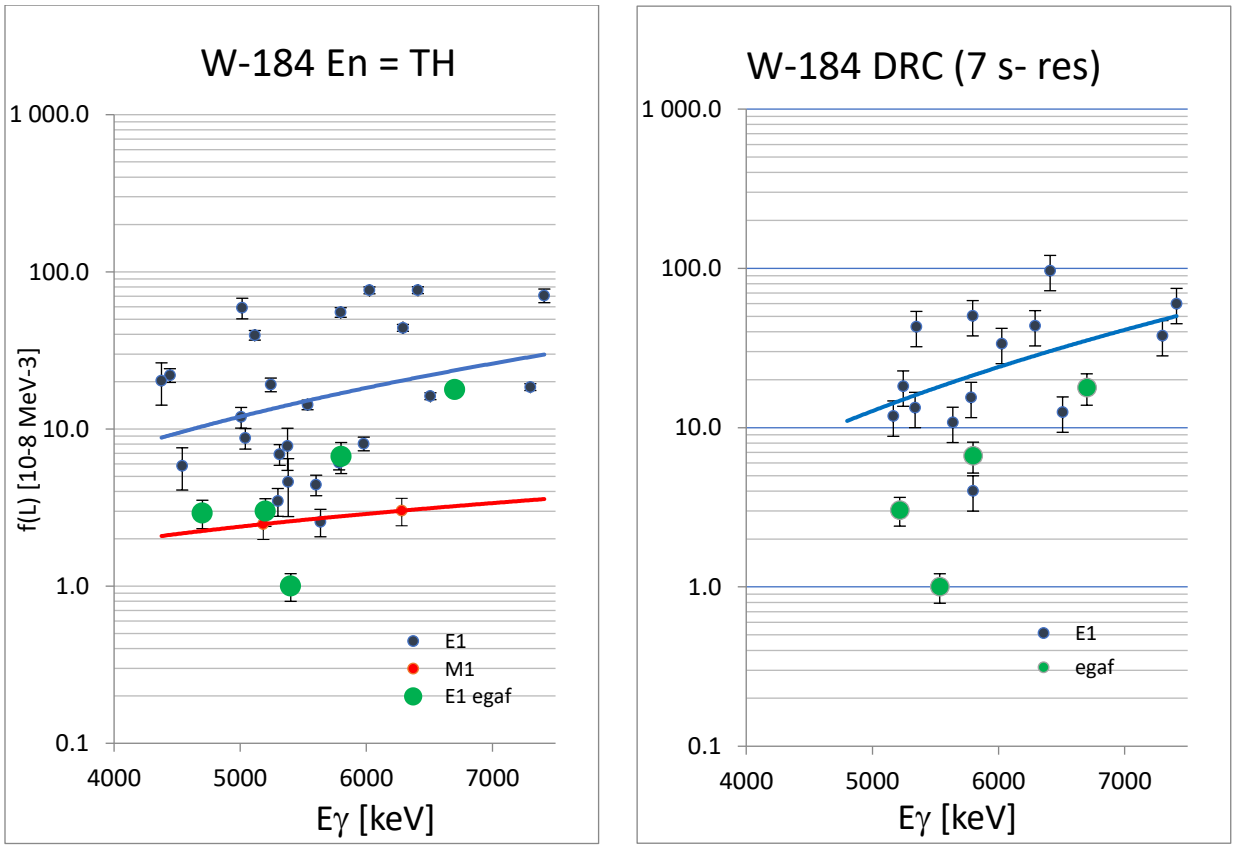

Fig.6 *Comparison of the THC f(L) ^{184}W data from the recent work and Ref. [9] with the <f(L)> DRC results from Ref. [3]. The green points are E1 data from the EGAF data base.*

Lu-177_ The original value of <<f(E1)>> = $3.23_{x}10^{-8}$ was found incorrect. The experimental averaged I_{γ} were taken from a preprint of the Dubna report and there the absolute intensity was given as I_{γ}/1000 neutrons and this was used in the Ref. [3]. In the official publication the intensity was given as per 100 neutrons and this introduced a normalization error of data in Ref. [3]. The newly evaluated DRC data are now in a good agreement with the THC and EGAF data as demonstrated in Figs. 7 and 8. The 177Lu outlier has moved from low to high value. The new <PSF> value introduced.

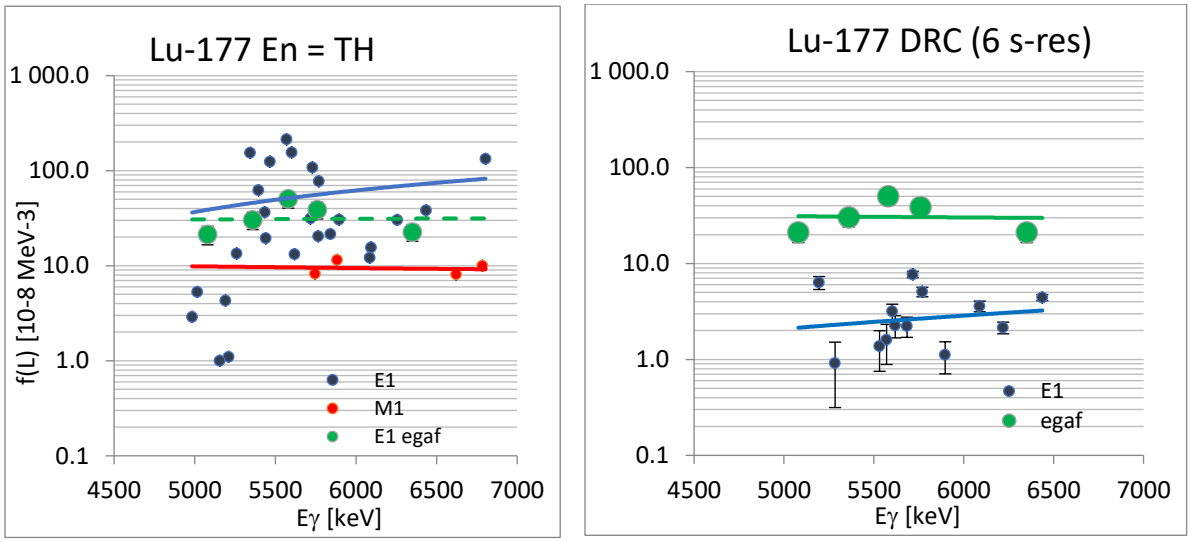

Fig.7 *Comparison of the THC f(L) ^{177}Lu data from the recent work and Ref. [9] with the <f(L)> DRC results from Ref. [3]. The green points are E1 data from the EGAF data base [9].*

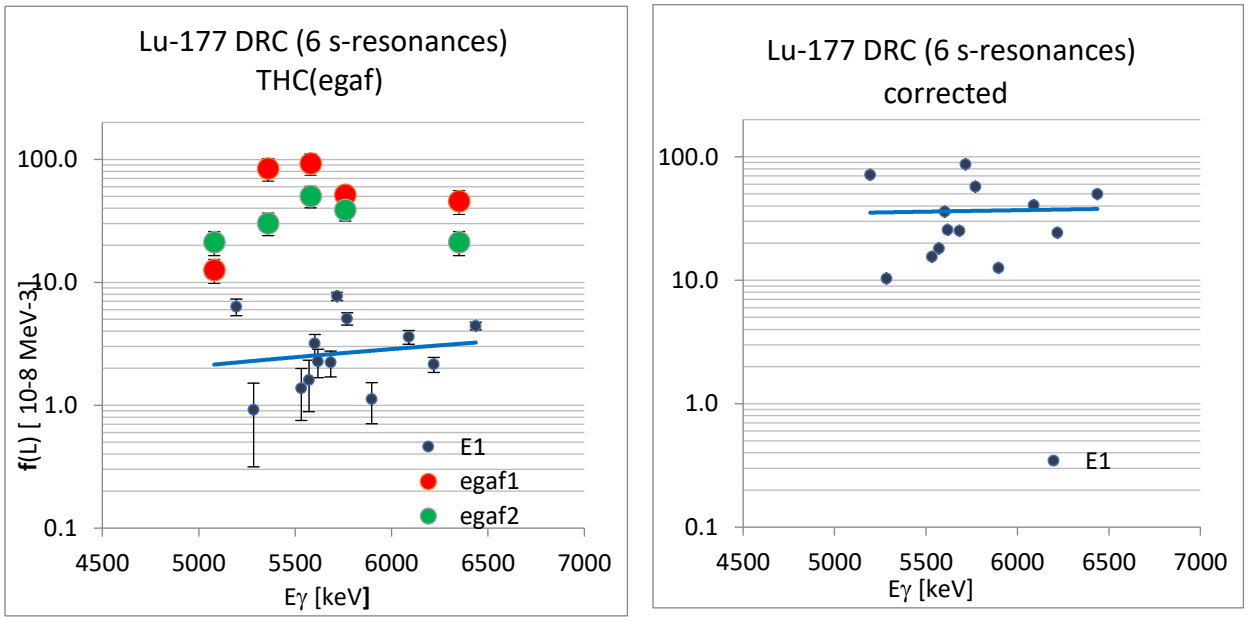

Fig.8 *Comparison of the THC f(L) ^{177}Lu <f(L)> DRC results from Ref. [3] with E1 data from the binned present THC data (red points) and the EGAF data base (green points). The righthand plot shows the newly corrected DRC data*

U-237 - The <Eγ> range of almost all actinide targets have energies between 3.5 and 4.5 MeV and a large re-normalization to the mean energy of 6.5 MeV, using the assumed E_γ^2 dependence, propagates the uncertainty and may disregard actinides for the systematics derivation. The sensitivity to this decision is tested bellow. An example of low energy <<f(L)>> data is shown in Fig. 9 for the ^{237}U nuclide. However, the E1 data reasonably agree with slope of the GDR systematic f(E1) prediction which suggest that the assumed E_γ^2 correction may give a representative extrapolation. This conclusion can be applied also to other actinide targets with $<E_\gamma> < 5$ MeV.

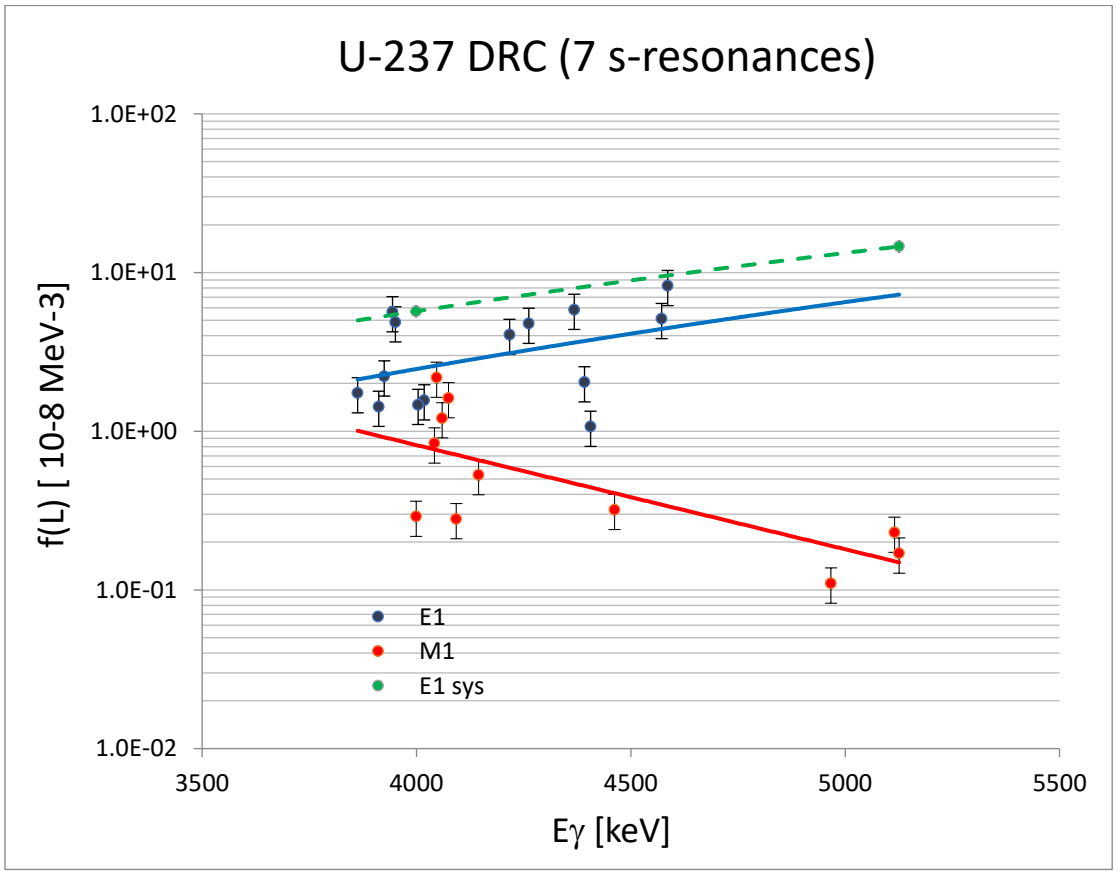

Fig.9 *The DRC f(L) ^{237}U data from Ref. [3]. Note the reasonable agreement of E1 data with the systematic prediction of the GDR down to the lower energies.*

3.2 E1 conclusions

The revision of the <<f(E1)>> values, used for the derivation of the PSF systematics equation at the energy of 6.5 MeV, included several changes. All outliers for targets with A > 50 have been inspected and their values validated by the comparison with the THC data. Further the ^{177}Lu entry was corrected. The influence of four actinide targets with $\langle E_\gamma \rangle$ below 4 MeV, not corrected for the E_γ dependence to 6.5 MeV, has been tested and the difference is shown in Figs. 10 and 11. The corresponding trend fits are $\langle\langle f(E1) \rangle\rangle = 0.003\ A^{1.62 \pm 0.30}$ and $0.002\ A^{1.72 \pm 0.30}$, respectively with and without actinides.

The influence of the adopted data with $\langle E_\gamma \rangle$ outside (6.5 ± 1.0) MeV have been tested applying the E_γ^2 dependence correction. The trend equation is by this slightly increased as shown in Fig. 12. If the entries with $\langle E_\gamma \rangle$ < 4.5 MeV are corrected by E_γ^2 dependence the trend equation underwent a relatively small change to $\langle\langle f(E1) \rangle\rangle = 0.002\ A^{1.65 \pm 0.30}$.

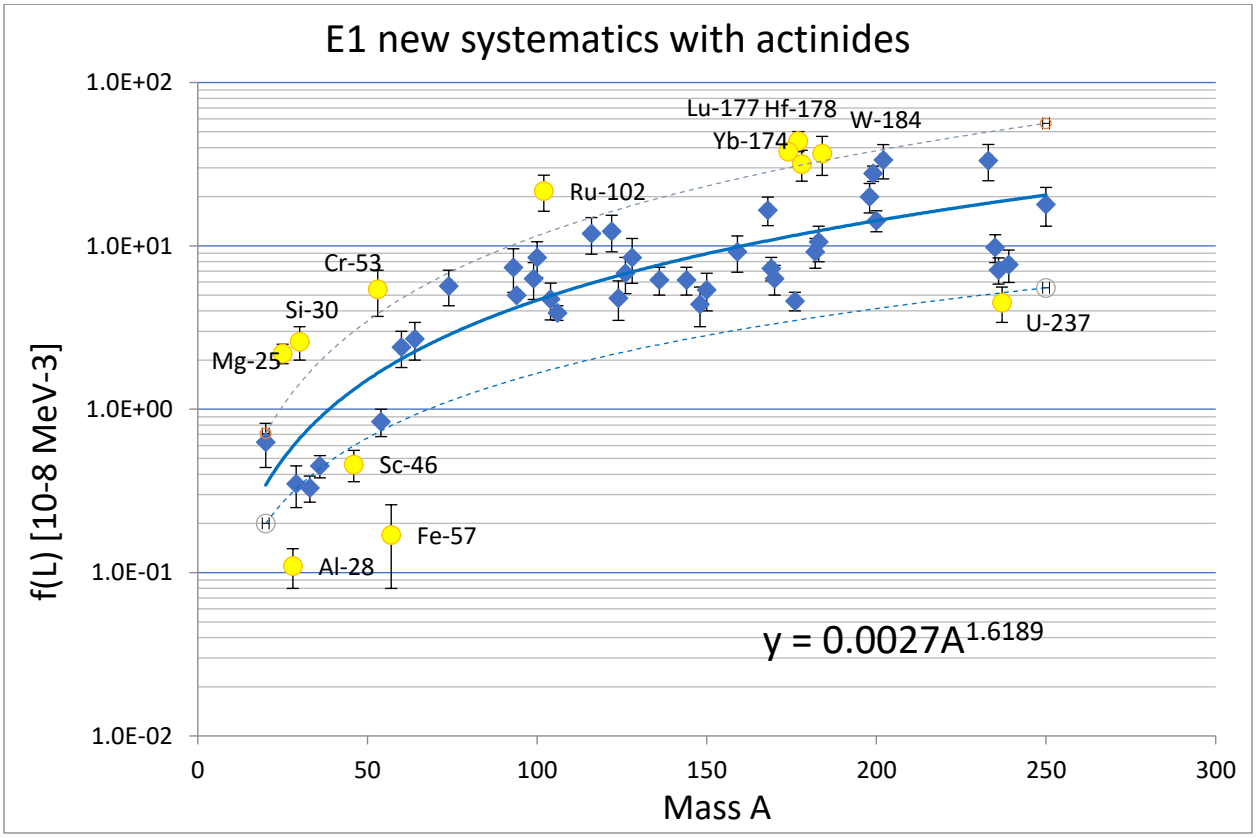

Fig.10 *Quasi-mono energetic doubly average strength functions <<f(E1)>> from recent re-evaluation with trend curve systematic as a function of the mass A. The dotted line is one SD dispersion from the assumed LSQ procedure. Data close or outside to dispersion curves have been added as the outlying data (yellow data points) with validated values. The influence of actinides (with $\langle E_\gamma \rangle$ bellow 4.5 MeV) is shown in the present and next two plots, this figure includes uncorrected values (for the E_γ dependence).*

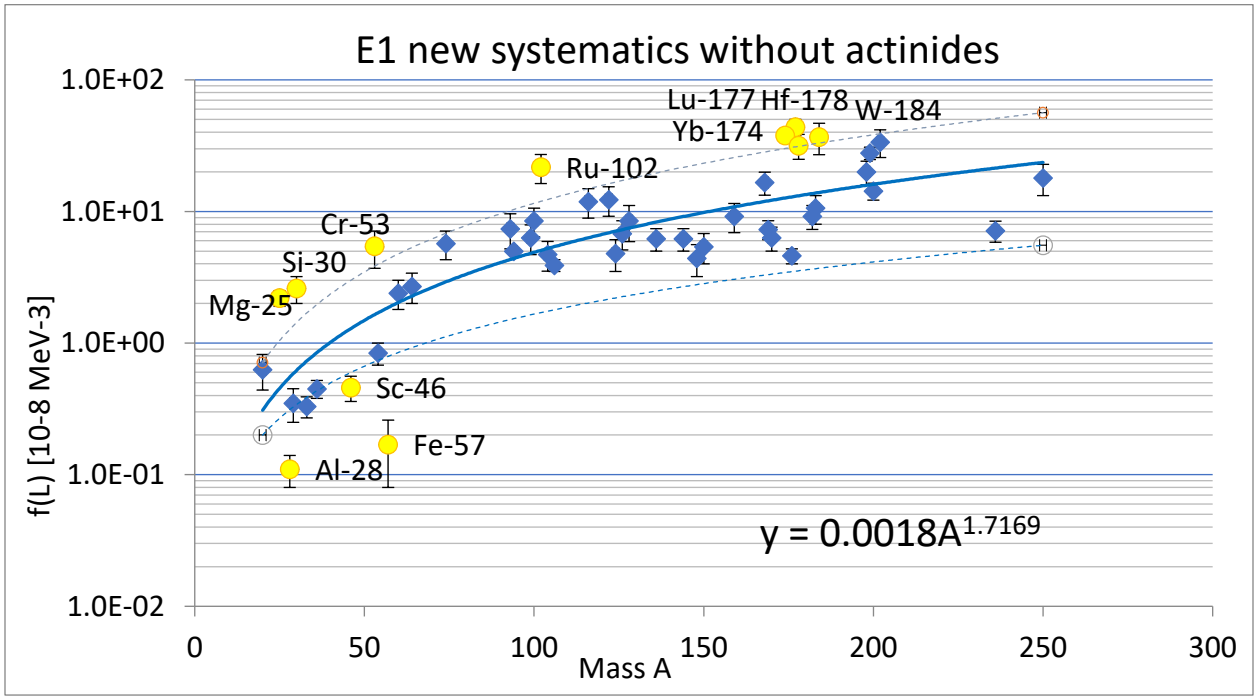

Fig. 11 *Quasi-mono energetic doubly average strength functions <<f(E1)>> from Fig. 10 processed without the original actinide data < 4.5 MeV.*

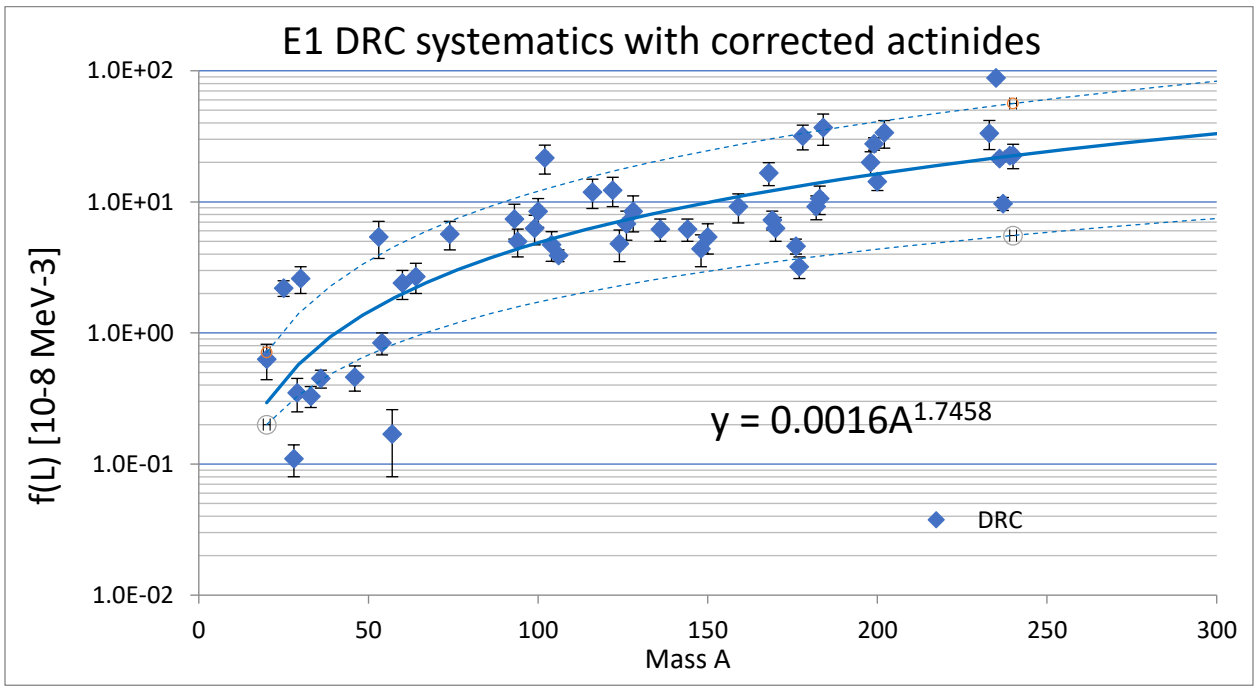

Fig. 12 *Quasi-mono energetic doubly average strength functions <<f(E1)>> from Fig. 10 with the actinide data corrected for the E_γ^2 dependence to 6.5 MeV.*

The original final equation from Ref. [3] <<f(E1)>> = 0.004 $A^{1.56\pm0.30}$ at $\langle E_\gamma \rangle \simeq$ 6.5 MeV has changed to the dependence between <<f(E1)>> = $0.003A^{1.62\pm0.30}$ at 6.3 MeV or <<f(E1)>> = $0.002A^{1.75\pm0.30}$ at 6.3 MeV, the spread is due to the influence of the actinide data at the end of the mass A region. The differences of these fits are graphically shown in Fig. 13.

This comparison shows that the difference between data samples without actinides and corrected actinides is marginal (see Fig. 13) and therefore their mean value is adopted as the recommendation for the f(E1) systematics

<<f(E1)>> = $0.002A^{1.73\pm0.30}$ at 6.5 $\pm$ 0.5 MeV.

The difference against the previous recommendation gives for targets with A > 100 values larger by 20 – 30%.

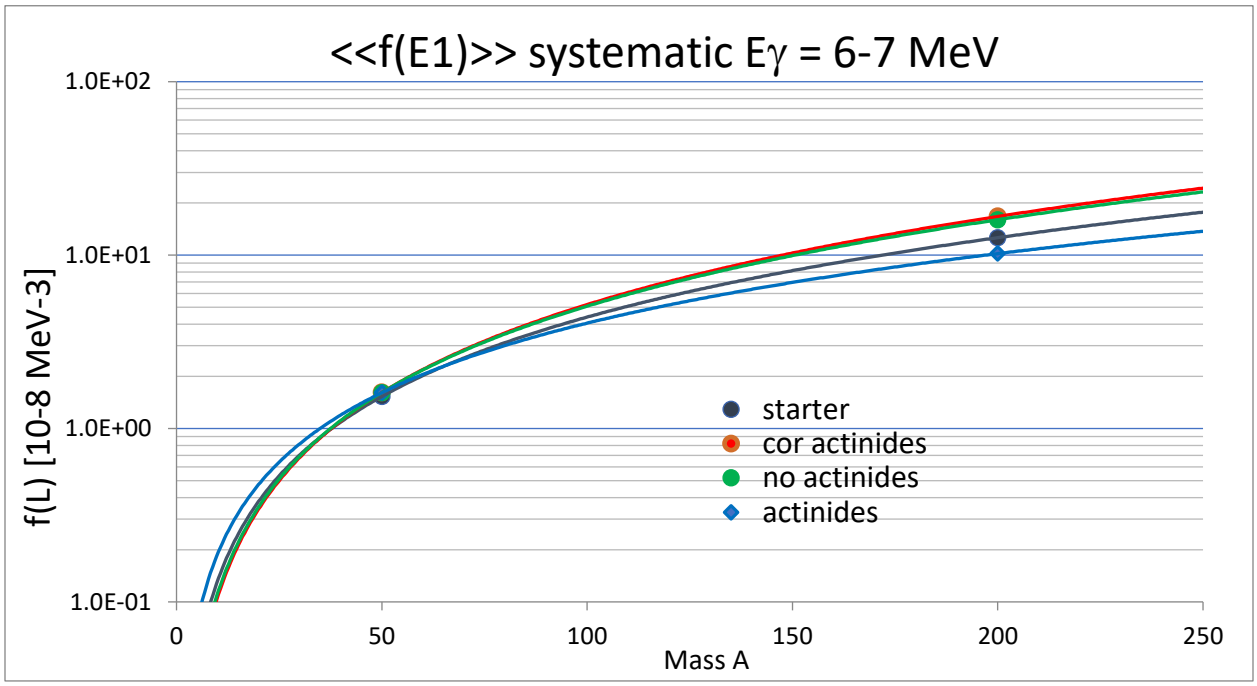

Fig. 13 *The development of the quasi-mono energetic doubly average strength functions <<f(E1)>> systematics over the period of last two years. Note the negligible difference between data sets without actinides and the E_γ corrected actinide values.*

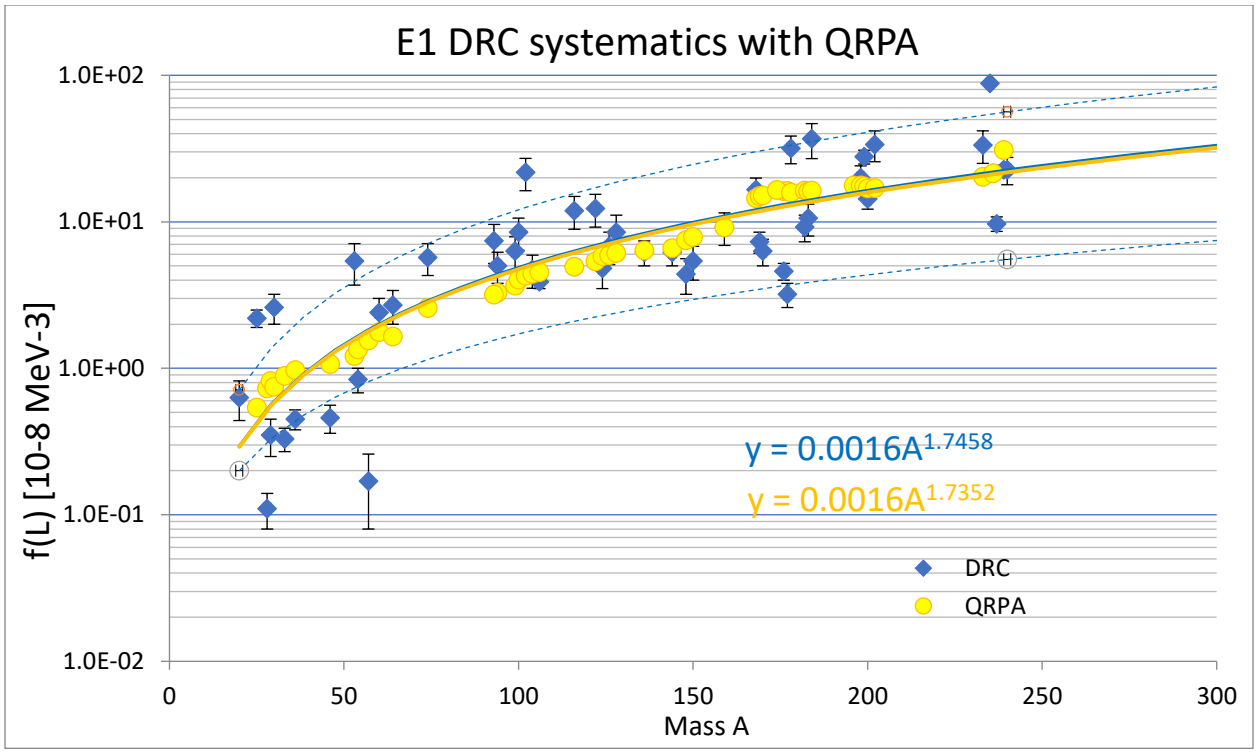

Fig. 14 *Quasi-mono energetic doubly average DRC strength functions <<f(E1)>> from Fig. 12 compared with the macroscopic D1M+QRPA predictions over the 6.5 ± 0.5 MeV region [6]. Note the excellent agreement of both trend curves.*

As two final tests we compared firstly the final E1 systematics with the theoretical predictions from the D1M+ QRPA model [6] over the energy range between 6 and 7 MeV of gamma-ray energy. The resulted data are shown in Fig. 14 and their trend fit equation compared with the final DRC data. The agreement is excellent which gives the additional support to the present DRC treatment and the inclusion of the corrected actinide data.

For the second test of the systematics we compare three independent PSF data sets from the DRC [3], THC [7] and EGAF [6,9] data bases. The DRC and THC data are averaged <f(E1)> values over the E_γ energy window (6.5 ± 0.5) MeV. The EGAF data base [6] has been processed in the PSF values by Firestone [9] and resulted in about 1500 binned E1 and M1 PSF values. The two thermal capture data sets (THC and EGAF) have been independently processed including the absolute calibration. However, the binning of the EGAF PSF data entries disables a direct comparison. In order to do so, we have selected from the EGAF file all data with $<E_\gamma>$ between 6 and 7 MeV and used them in the comparison with the averaged <6.5> MeV DRC/THC data shown in Fig. 15.

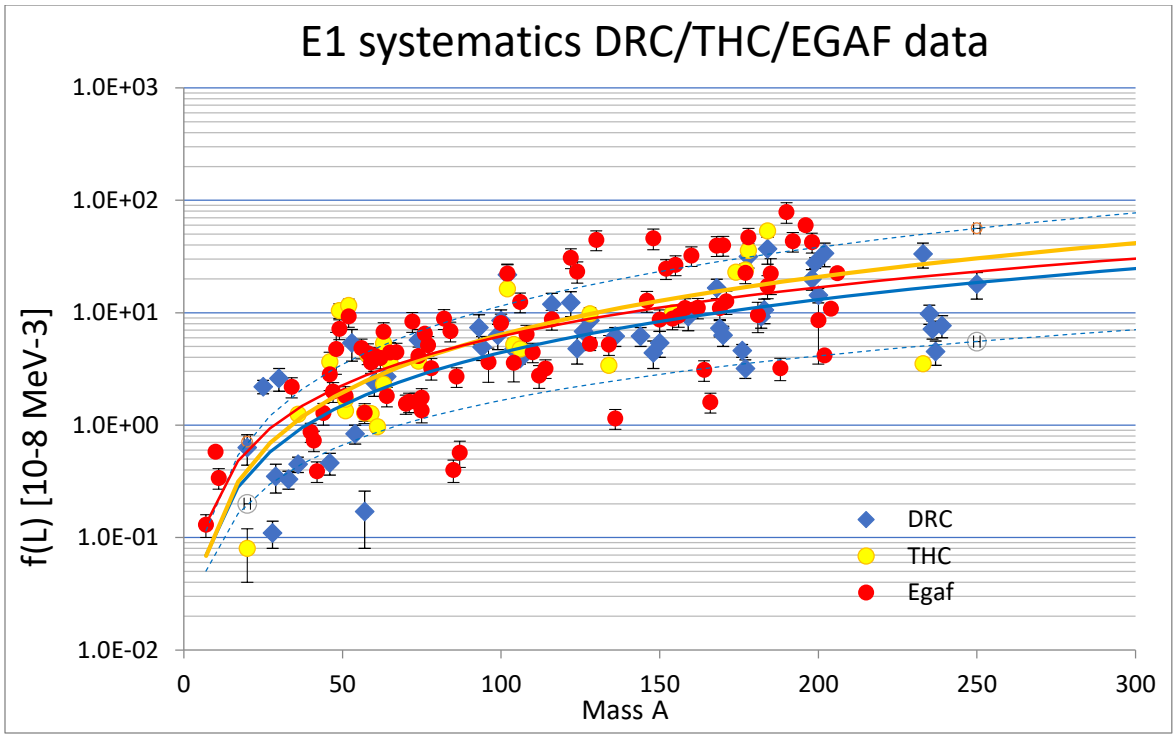

Fig.15 *Quasi-mono energetic doubly average strength functions <<f(E1)>> from recent evaluations using DRC data (blue points) [3] and thermal data from THC (yellow points) [7] and EGAF(red points) [9], respectively. The fitted trend curves are power mass A dependent. The dotted line is one SD dispersion from the LSQ procedure of the DRC data (see Fig.2) which have the smallest Porter-Thomas fluctuations.*

Note a rather good agreement of all curves fitting three independent data collections in terms of the origin, data processing and the absolute calibration. It seems that the data dispersion is averaged out, if large number of data points is used, and the result is close to the real situation. The dispersion of the DRC data is narrower as expected from the far better averaging. Remark on the EGAF data base, two significant errors in the applied D_o values have been spotted (for ^{76}As and ^{148}Sm) and corrected.

3.3 M1 – DRC outliers

The M1 systematic equation has not been considered in Ref. [4] as a normalization tool but only as an additional information. The reason for this decision was based on the lower statistical accuracy with large spreading of the data and further because there was no simplified modelling of the energy dependence, due to the increased complexity of the M1 collective excitations. The starter for the present revision is the quasi-mono energetic double average strength functions <<f(M1)>> data base from Ref. [4] (see Fig.16).

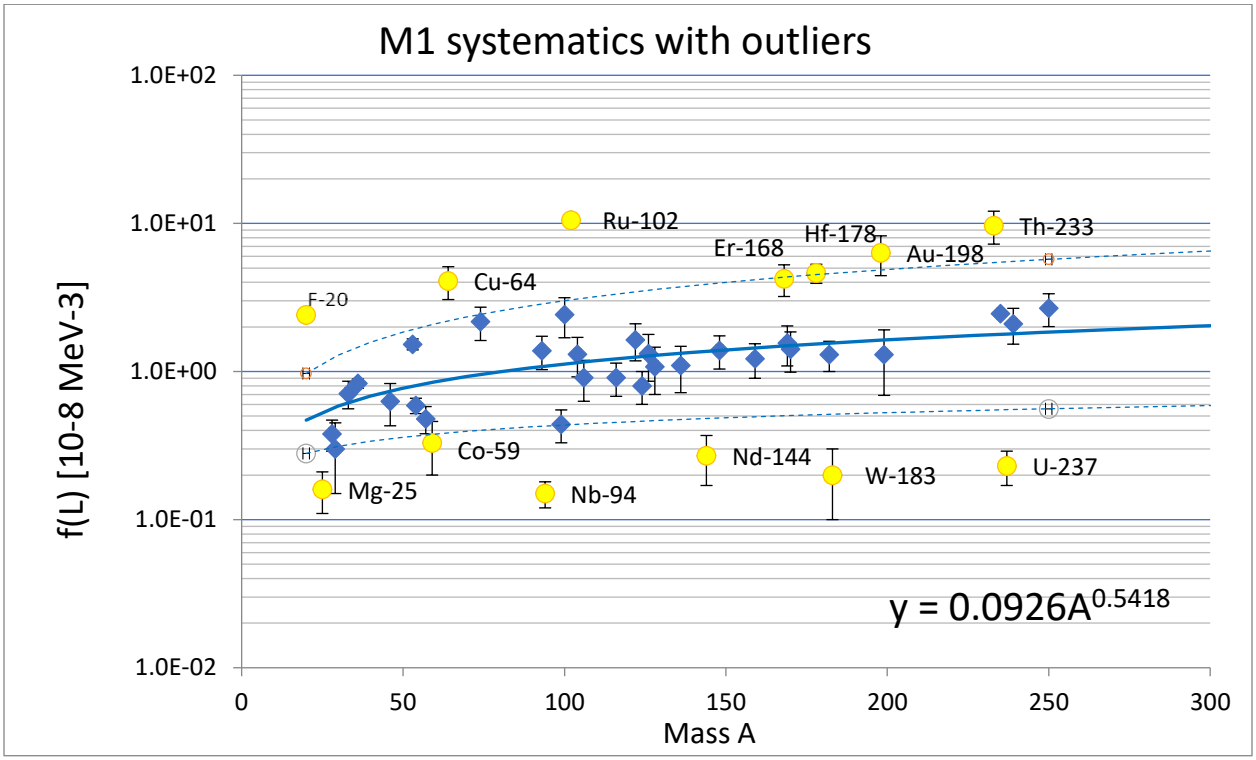

Fig.16 *Quasi-mono energetic doubly average strength functions <<f(M1)>> from Ref. [4] with trend curve systematic as a function of the mass A. The dotted line is one SD dispersion from the LSQ procedure. Data close or outside to dispersion curves have been added as the outliers (yellow data points).*

The experimental ($E_\gamma \pm \Delta E_\gamma$) energy window used for the derivation of the systematics for the M1 transition is shown in Fig. 17, where the mean E_γ values are plotted as a function of A. The values of $<E_\gamma>$ are more often, compared to the E1 data, outside the 6 – 7 MeV band, which may introduce an additional uncertainty in the derived PSF values. The rather low values of $<E_\gamma>$ for the actinide targets were not considered, because they may bias the systematic through the influence of the decrease of the spin-flip resonance. Other heavily deviating nuclides are ^{33}S and ^{106}Pd, with mean $<E_\gamma>$ energies close to 4 and 8 MeV. No systematic energy dependence of the energy E_γ below the spin-flip energy is available and therefore no correction could be applied.

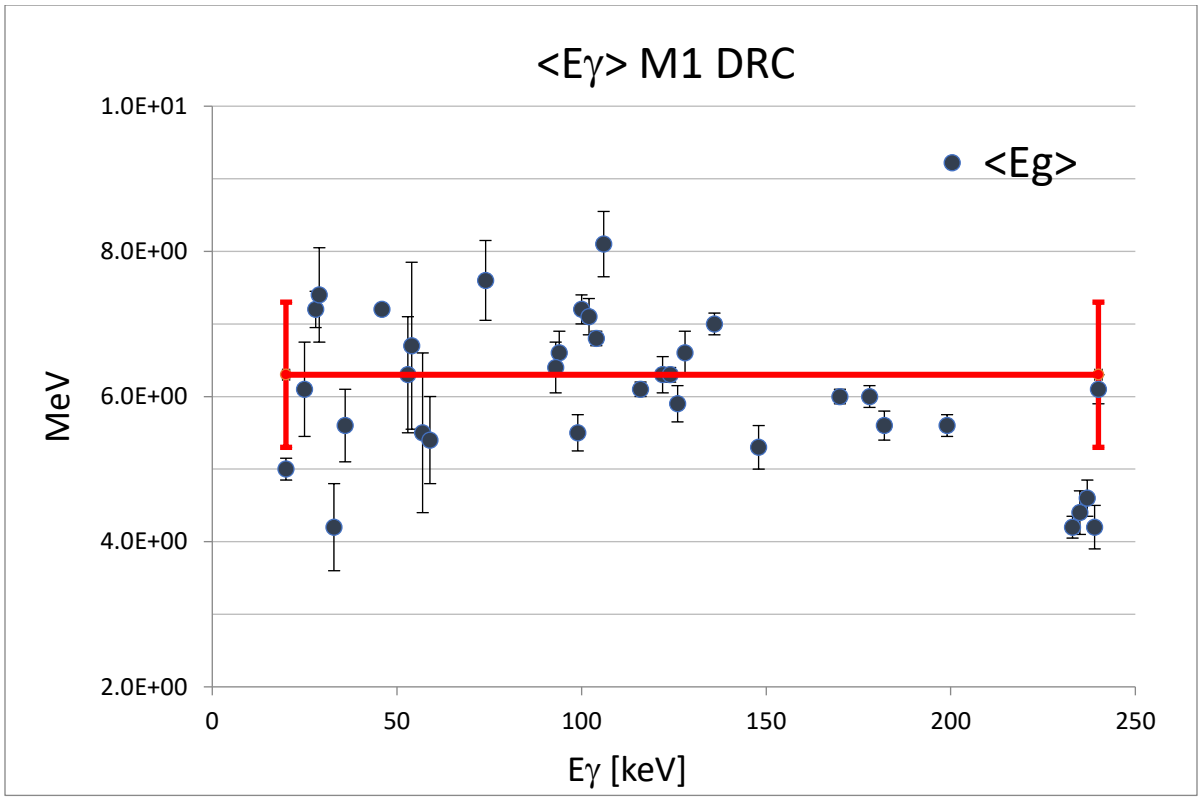

Fig. 17 *The mean energy regions ($E_\gamma \pm \Delta E_\gamma$) of the THC data used to generate the double average <<f(L)>> values for the systematic equation. The red curve indicates the mean value of 6.3±1.0*

Single M1 transition cases: The original data base, used in Ref. [4], also included nuclides with only one M1 transition, which without averaging may fall significantly off the main trend. Such entries have been neglected in the present analysis (^{64}Cu, ^{144}Nd, ^{183}W and ^{198}Au). For the ^{64}Cu nuclide one transition was incorrectly assigned as M1 (E_x = 1322 eV $J_f = 3^-$ recently changed in ($1^+2^+3^+$) spin assignment and so only one M1 transition remains.

Co-59 – The ^{59}Co data point was incorrectly assigned in the plot legend and should be ^{59}Fe. The <<f(M1)>> value is based on the averaging of 2 p-wave resonances and there is a large uncertainty of the Γ_γ radiation widths. Using the mean $\langle\Gamma_\gamma\rangle_p$ value the outlying value is increased and now reasonably fits the trend. Consequently, the ^{59}Co legend has been removed from the plot.

Ru-102 – The E1 and M1 strengths in all the measurements confirmed, and with the DRC, the THC and the EGAF data all in good agreement (see Fig. 18) it can be concluded that the ^{102}Ru PSF is outlying the trend dependence purely due to statistical fluctuations. The deviation from the GDR model seems too improbable. The DRC value is maintained.

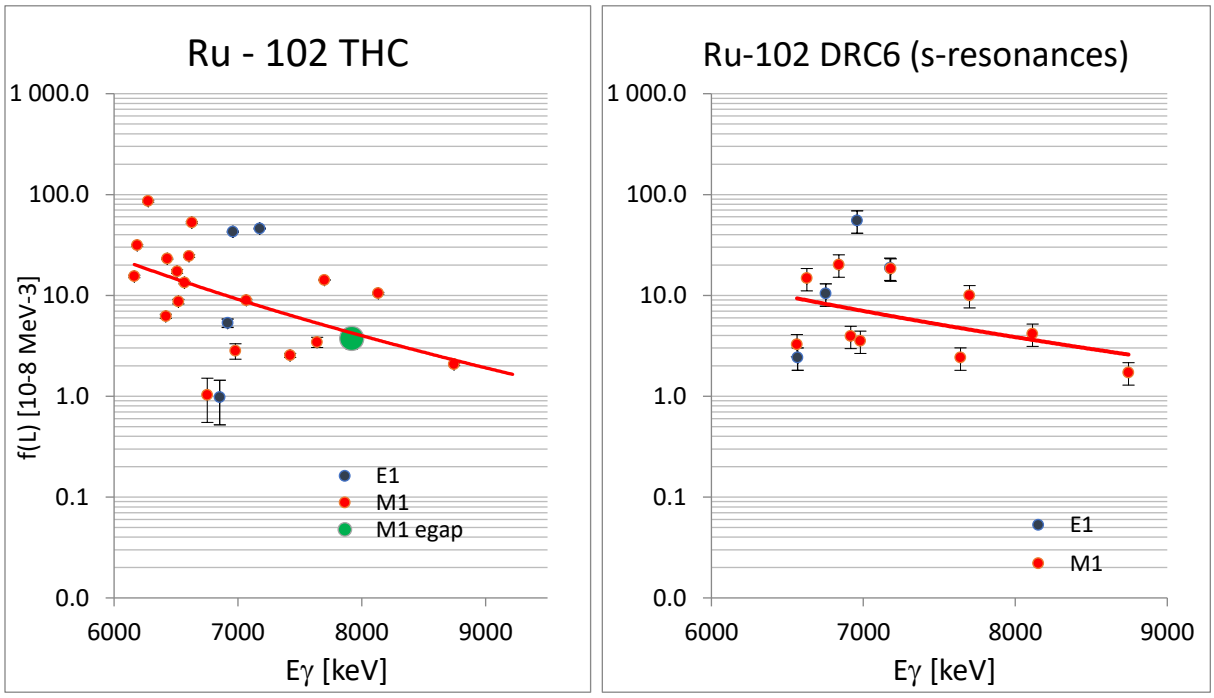

Fig. 18 *Comparison of the f(L) ^{102}Ru <f(L)> DRC results from Ref. [4] with M1 data from the present THC work (red points) and the EGAF data base (green point). The righthand part of the figure shows the DRC data.*

Er-168 – The EGAF E1 and M1 data points are in an agreement with the well averaged (81 resonances) E1 and M1 DRC data (see Fig. 19). The scatter of the E1 EGAF data is rather large but the mean value trend is close to the DRC data. The M1 data are in a rather good agreement. Based on this comparison we consider the DRC <<f (E1, M1)>> values to be confirmed.

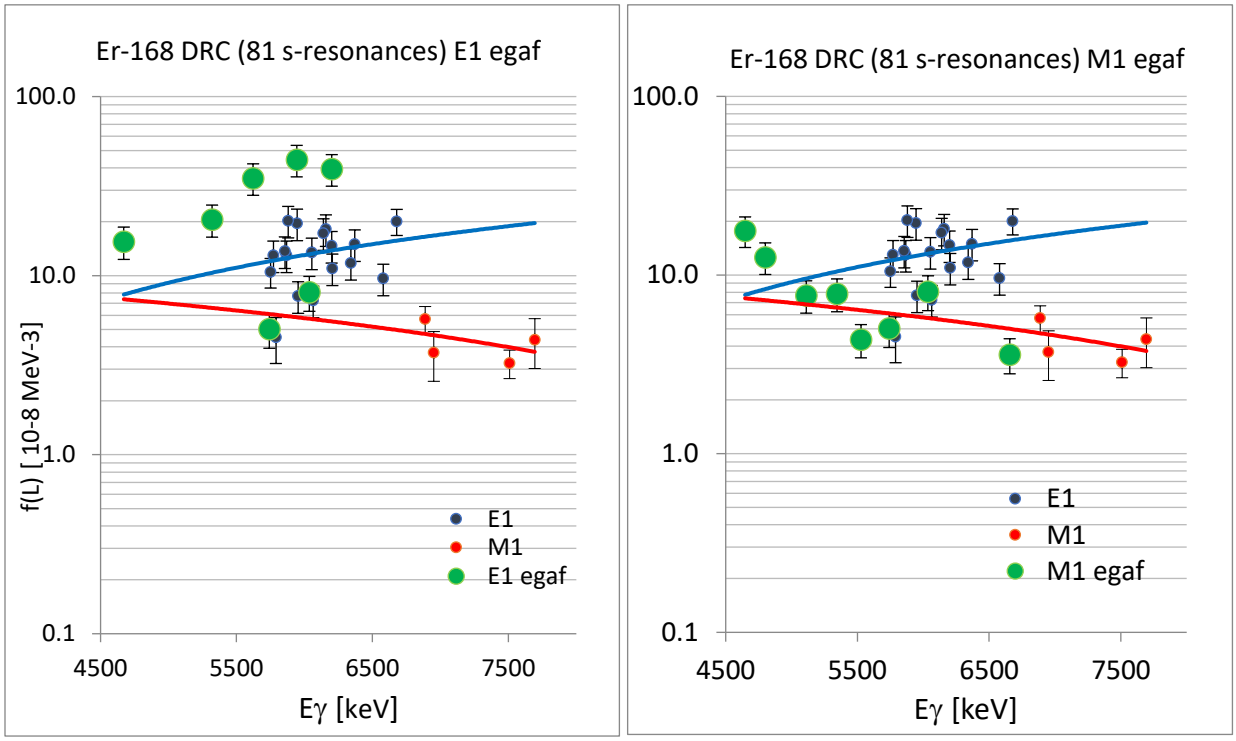

Fig. 19 *Comparison of the ^{168}Er <f(L)> DRC results from Ref. [4] with E1 and M1 binned thermal capture data from the EGAF data base (green points).*

Hf-178 – No THC evaluation is available and only EGAF binned thermal data can be used for the comparison. The EGAF E1 data points are in a good agreement with the well averaged (20 resonances) E1 DRC data (see Fig. 20). However, the M1 data are problematic. Based on this comparison we consider the DRC <<f (E1, M1)>> values to be confirmed.

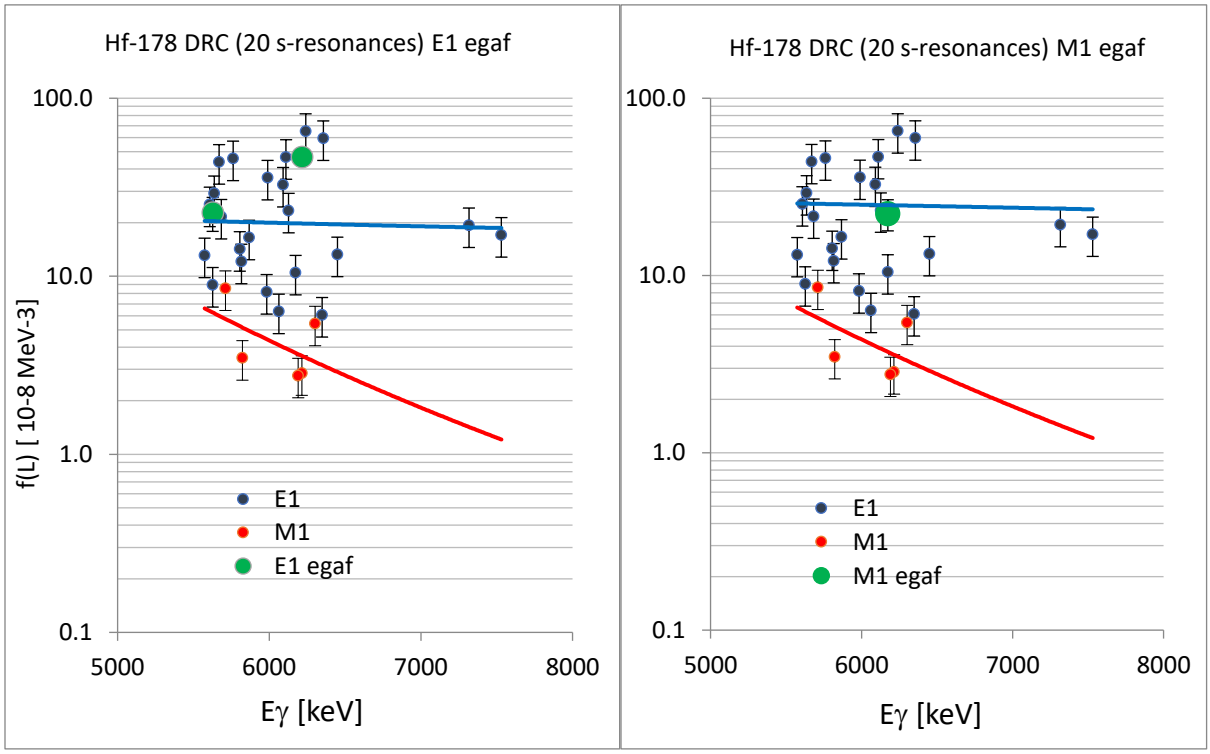

Fig. 20 *Comparison of the ^{178}Hf <f(L)> DRC results from Ref. [4] with E1 and M1 binned thermal capture data from the EGAF data base (green points).*

Nb-94 – The robust BNL chopper data [12] have been chosen for the ^{94}Nb DRC data. In the analysis are the E1 data are taken from four p-wave resonances and the identical transitions are used as M1 transitions from the three s-wave resonances. A calculation error of the DRC <<f(E1,M1)>> values_has been spotted in the averaging part of the previous analyses and the corrected data are now shown in the Appendix. This error was responsible for the outlying <<f(M1)>> value which has now been corrected, also the E1 data have been checked and the resulting agreement with the THC data is shown in Fig. 20

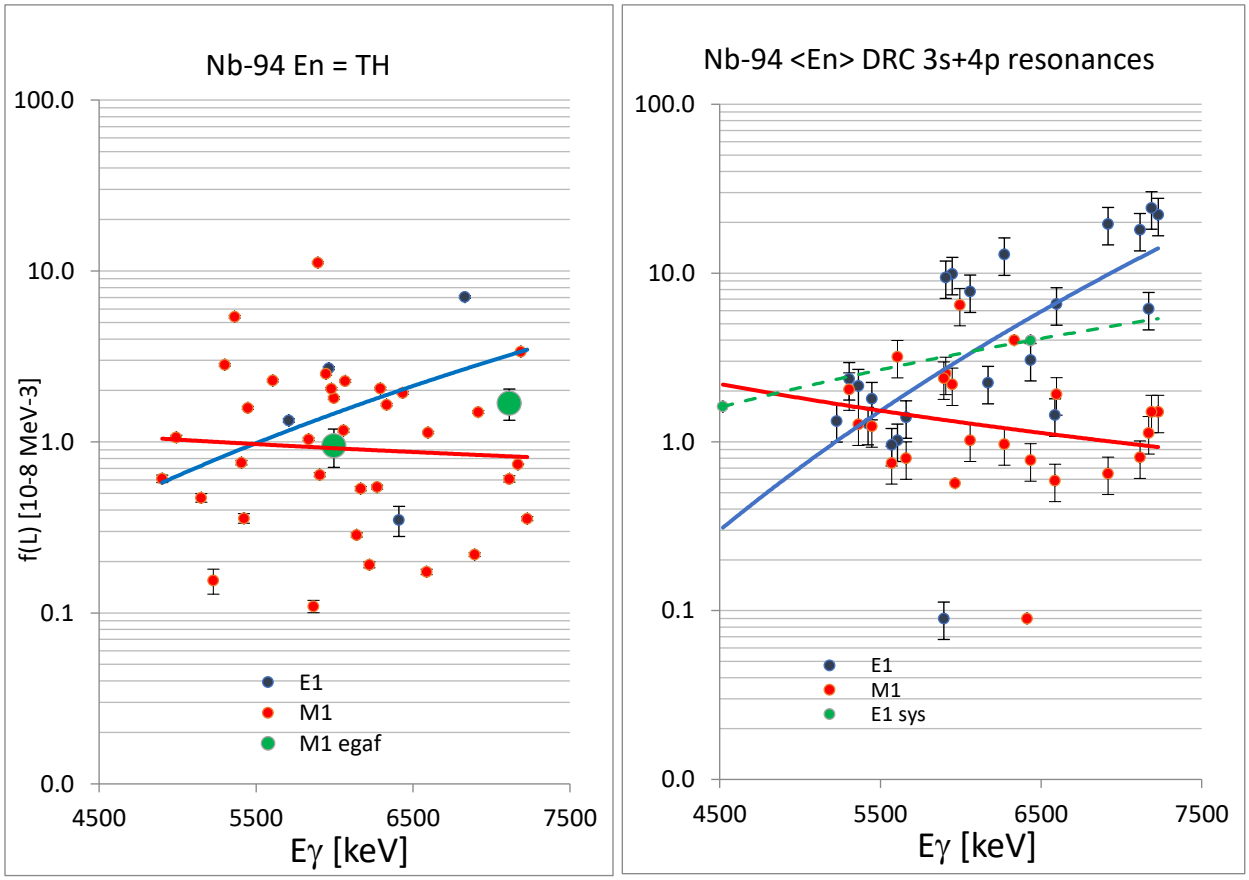

Fig. 20 *Comparison of the f(L) ^{94}Nb <f(L)> corrected DRC results with M1 data from the present THC work and the EGAF M1 data (green points). The righthand part of the figure shows the revised DRC data of Ref. [4] (see the Appendix).*

Th-233 and U-236 – All actinides except for ^{240}Pu have an <E_γ> value < 4.5 MeV and therefore they have been neglected as entries for the <6.5> MeV systematics. The correction for the energy dependence has not been considered based on previous discussions.

3.4 M1 conclusions

The revision of the <<f(M1)>> values included the inspection of outliers for targets with A > 50 by comparison with the THC data. Firstly, entries based on only one transition have been removed (^{64}Cu, ^{144}Nd, ^{183}W and ^{198}Au). The erroneously used ^{59}Co symbol was corrected to ^{59}Fe and its value no longer has the outlier status. The influence of the adopted data with $<E_\gamma>$ outside (6.5 $\pm$ 1.0) MeV is for M1 transitions is relevant only for actinide targets. Because no theoretical E_γ dependence correction is available, only ^{240}Pu data are considered and the ^{233}Th and ^{235,237,239}U data points have been removed. The three remaining outliers ^{102}Ru, ^{168}Er and ^{178}Hf have been confirmed as correct values, while only for ^{102}Ru are both the E1 and M1 data a real problem to understand (see the discussion above). Further the ^{94}Nb entry was corrected. The influence of four actinide targets with $<E_\gamma>$ below 4 MeV, not corrected for the E_γ dependence to 6.5 MeV, has been tested and the corresponding trend fits are <<f(M1)>> = 0.064 $A^{0.63\pm0.18}$ and 0.063 $A^{0.65\pm0.18}$, respectively with and without actinides. The influence of the actinide targets with $<E_\gamma> \leq 4.5$ MeV is negligible but it was still decided to include only one actinide, ^{240}Pu with energy $<E_\gamma>$ = 6.2 MeV, and the resulting curve is shown in Fig. 21.

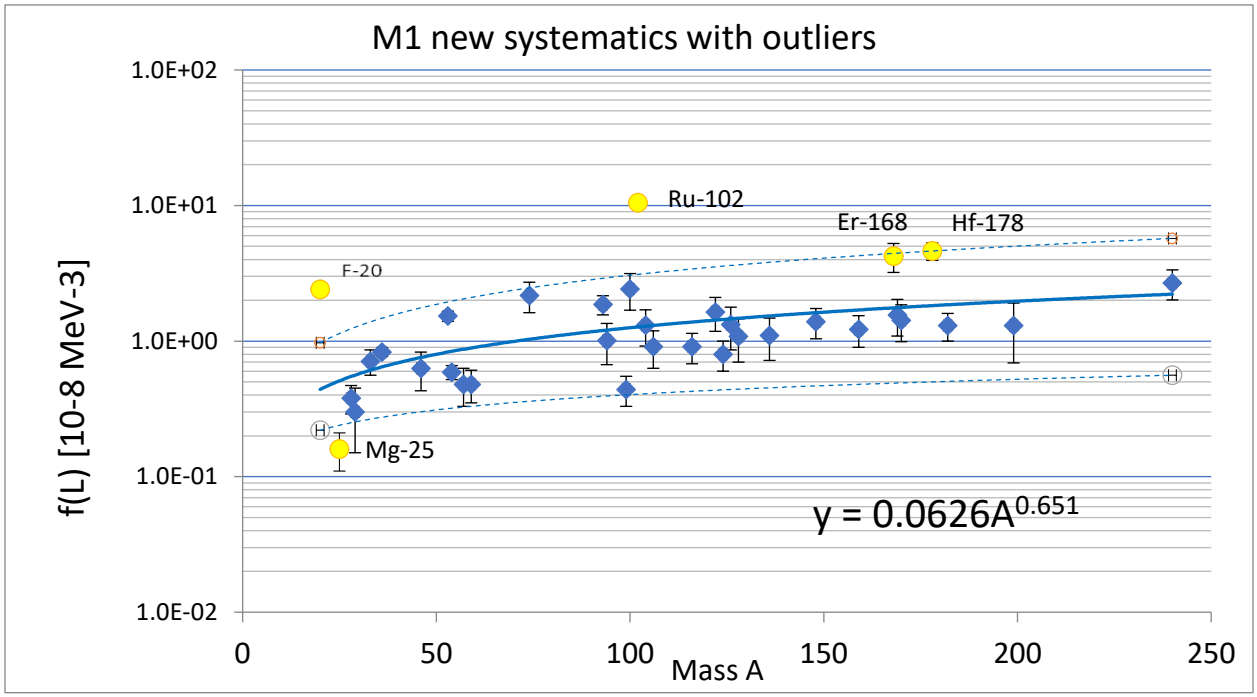

Fig. 21 *Final quasi-mono energetic doubly average strength functions <<f(M1)>> from Fig. 10 processed without the original actinide data < 4.5 MeV. The basis forms the same data as in Fig. 16 with all corrections and removals implemented. Note a rather smooth data trend above A > 100.*

The M1 mass dependence, contrary to the E1 radiation, has no analytical formulation and may be understood as a crude representation of a complex situation. The energy window of <6.5 MeV> falls in between the slopes of the spin flip resonance and of the scissors-mode (see Ref. [11]). The

mass dependence of both these excitations, is discussed in terms of simplified analytical expressions of their peak strength and for both modes is predicted as ~ A^1. This explains, in a reasonable agreement with the present ~$A^{0.65}$ value, the increasing strength for increasing A. The simple empirical partial SMLO M1 prediction, from the family of Lorentzian based approximations, describes the f(M1) dependence on the energy E_γ and an example is shown in Fig. 22, taken from Ref. [11].

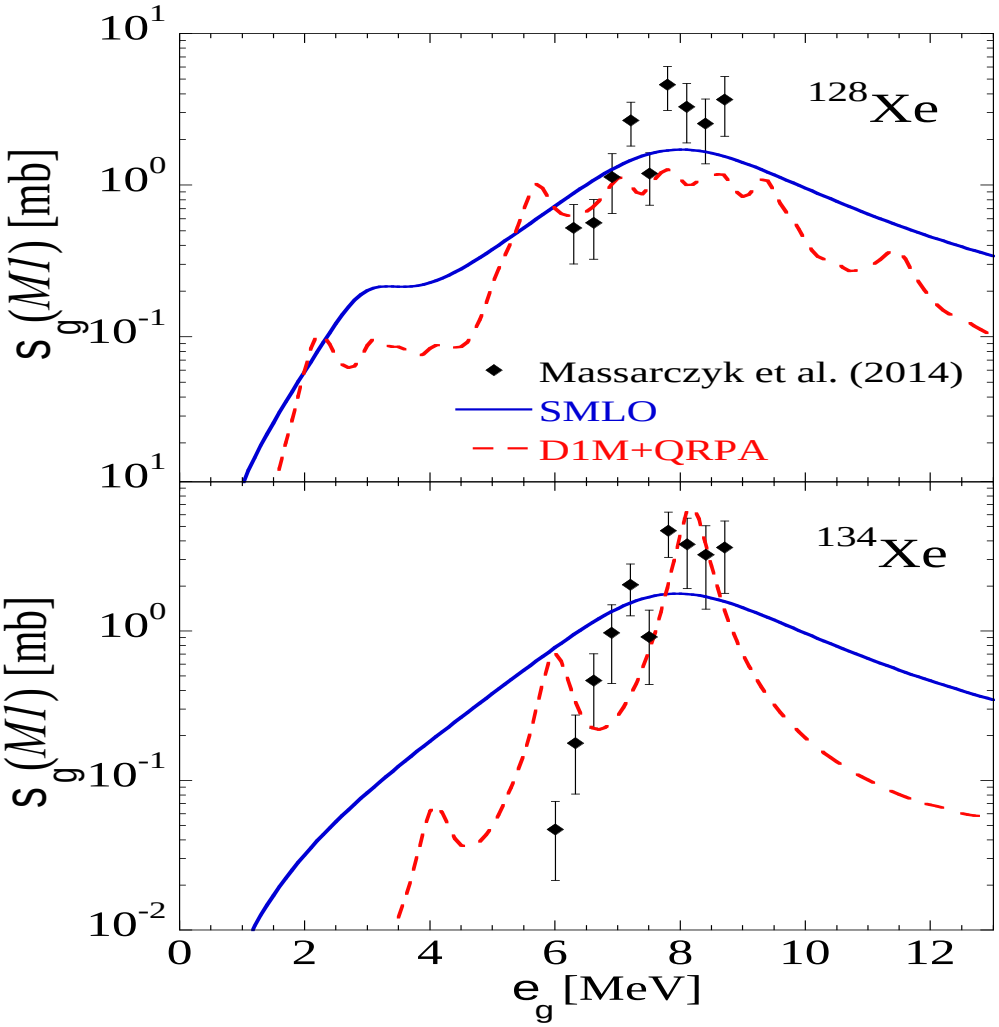

Fig. 22 *Comparison D1M + QRPA and SMLO M1 strength functions for the photo-absorption cross sections of ^{128}Xe and ^{134}Xe. Note the difference of the shape between scissors and spin-flip modes for spherical and deformed isotopes. Figure is adopted from Ref. [11].*

The recommended systematics prediction, for E_γ energies between 6 and 7 MeV, is given the equation

$$<<f(M1)>> = 0.063\ A^{0.65\pm0.18}$$

and is the one adopted. The uncertainty of the exponent indicates the statistical error, 1 SD of the LSQ fit, assuming the experimental data fluctuations follow only the normal distribution. The difference compared with the previous recommendations is rather small and for targets with A > 100 gives an increase of about 20 – 30%, see Fig. 23.We may conclude that for both E1 and M1 gamma rays the previous and present trend systematic remain rather close, justifying the present final recommendations.

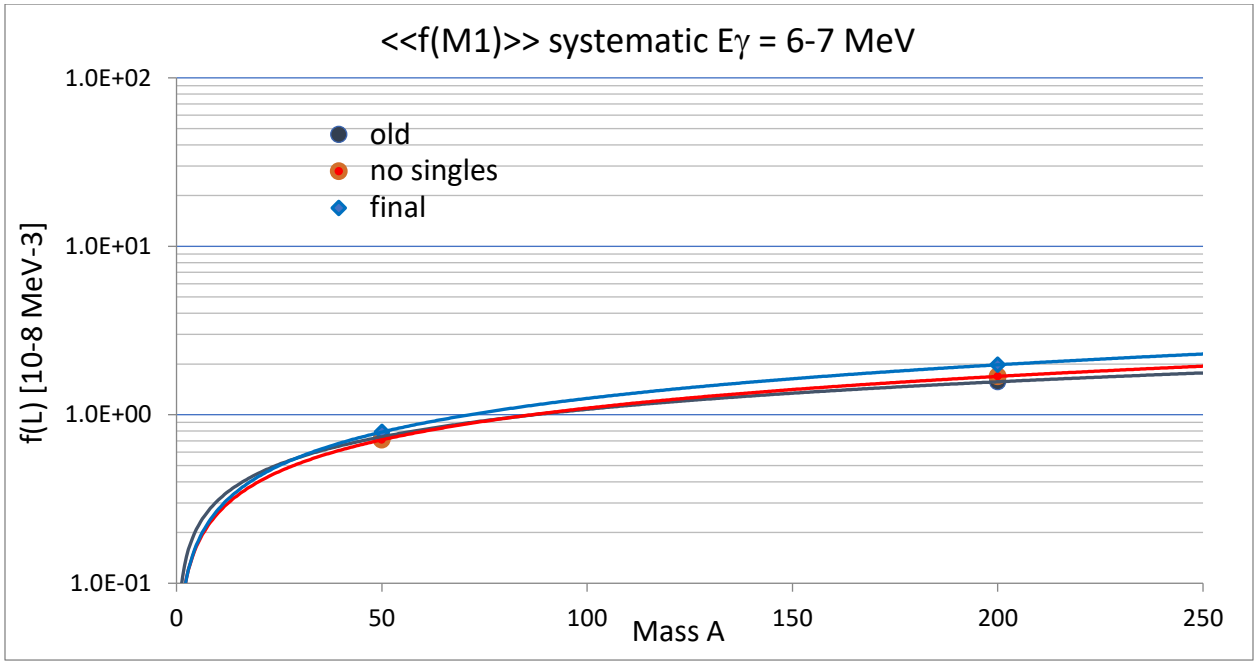

Fig. 23 *The development of the quasi-mono energetic double average strength functions <<f(E1)>> systematics over the period of last two years. Note the negligible difference between data sets without actinides and the E_γ corrected actinide values.*

As the last test we compared the final systematics with the theoretical predictions from the QRPA model, using the macroscopic calculations averaged over the energy range between 6 and 7 MeV of the gamma ray energy [11]. The comparison is shown in Fig. 24 and includes the QRPA trend compared with the final DRC data. The data show a rather significant difference between DRC data and the theory, especially for nuclides below A $\simeq$ 100. This is demonstrated by the two rather different trend equations, assuming the smooth mass dependence for data entries

$$<<f(M1)>>_{DRC} = 0.062\ A^{0.65} \text{ and } <<f(M1)>>_{QRPA} = 0.002\ A^{1.26}.$$

The smooth mass dependence of the QRPA data is a certainly a crude assumption because the theoretical prediction is heavily influenced by differences in M1 excitations between the spherical and deformed nuclei (see Fig.22) and may vary significantly within the 6-7 MeV energy range. The QRPA mass dependence of $A^{1.26}$ is rather close to the A^{1} used in Ref. [11] since the SMLO M1 systematics has been inspired from QRPA calculations. However, the main problem is the general underestimation of the experimental data by the QRPA theory, which remains unexplained and is an open question. It should be recalled that the D1M+QRPA strength correspond to the photo-absorption strength and not to the de-excitation one. The latter may differ from the former at low energy, especially for light A<100 nuclei, as discussed in Ref. [7,11]. The validity of the DRC input is supported by the excellent agreement of the E1 data with the theory, which supports the DRC data processing.

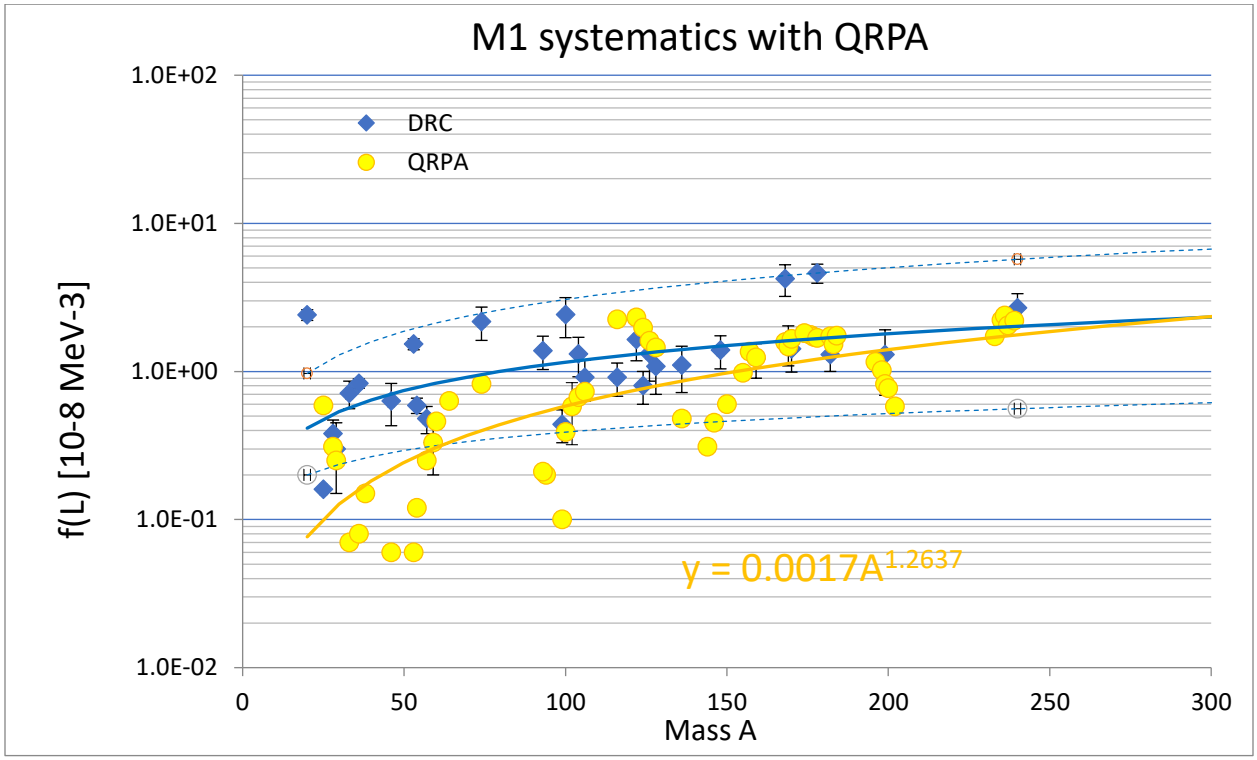

Fig. 24 *Quasi-mono energetic doubly average DRC strength functions <<f(M1)>> from Fig. 21 compared with the QRPA predictions of macroscopic calculations over the 6.5 ± 0.5 MeV region [10]. Note the overestimation of the DRC data trend for nuclides with A < 100. The QRPA predictions reveal a broad fluctuating structure responding to spherical a deformed target-nuclides with the inclusion of the scissors mode for deformed nuclei and the phenomenological zero-limit contribution to the de-excitation PSF [7].*

The thermal capture PSF data have been added to the <6.5 MeV> recommended data base and the extended listing is given in Table 4 and their intercomparison is graphically shown in Fig. 25. In

this figure three independent PSF data sets from the DRC [4], THC [8] and EGAF [7,10] data sets are compared in the same way as for the E1 data (see E1 Section). From the EGAF file we have selected all data with $<E_\gamma>$ between 6 and 7 MeV. The THC and EGAF data show much larger fluctuation compared to the DRC data, which can be explained by much poorer averaging in these experiments. However, the fitted trend lines, despite the crudeness of assumed power dependence, have a similar shape.

Table 4 Evaluation of the quasi-mono energetic strength function f(L) with three and more E1 and M1 transitions extracted from the DRC and THC (in blue) data. The DRC data corrected in the present work are printed in red, "na" stands for results taken from other references (no differential data available).

#res - number of included resonances with their l_n assignment
s(th) - thermal capture state
Spacing - spacing used for the evaluation
Do, D1 - spin independent spacing with corresponding <f(L)> values
(Do) - estimated, no value quoted in Ref. [9]
Do^J $D1^J$ - estimated spin dependent value of the spacing D_0 and D_1 for the spin J
<f(L)/d(L)> - the average PSF value with the statistical uncertainty
$<E_\gamma>/\Delta$ - mean energy $E_\gamma \pm \Delta$ of the 2Δ window

Nuclide product	**# res**	**Spacing**	**<f(E1) (d<f(E1)>)**	**$<E_\gamma>/\Delta$**	**<f(M1) (d<f(M1)>)**	**$<E_\gamma>/\Delta$**
		eV	**$*10^{-8}$ MeV^{-3}**	**MeV**	**$*10^{-8}$ MeV^{-3}**	**MeV**
F-20	2(p)	D1=60000	0.63(20)	4.6/2.0	2.41(23)	5.0/0.3
	s(th)	Do= (343000)	0.075(8)	5.2/1.0	0.13(3)	5.9/1.0
Mg-25	1(p)	$D1^{3/2}$=237000 D1 = 158000	2.21(30) 3.32(45)	6.1/1.3		
	1(d)	$D2^{3/2}$=220000 D2 = 110000			0.16(3) 0.32(6)	6.1/1.3
	s(th)	Do= (709000)			0.06(2)	6.5/0.2
Al-28	1(s)	Do^3=90630 Do =53000	0.11(3) 0.19(5)	6.6/1.1		
	1(p)	$D1^3$=97412 D1 = 28400			0.38(9) 1.3(3)	7.2/0.5
	s(th)	Do=53000			0.14(2)	6.4/0.2
Si-29	1(d)	$D2^{5/2}$=136800	0.35(10)	2.8/0.7	0.30(3)	7.4/1.3

		D2 = 64800	0.74(21)		0.63(7)	
	s(th)	Do=337000			0.013	6.6/0.6
Si-30	1(p)	$D1^2$=94320 D1 = 52400	2.59(56) 4.66(101)	6.3/0.4		
	s(th)	Do= (339000)			0.010(4)	6.8/0.3
S-33	1(p)	$D1^{3/2}$=138900 D1 = 46300	0.33(3) 0.99(9)	7.5/1.2	0.71(13)	4.2/1.2
	s(th)	Do= 179000			0.04(1)	7.2/0.6
Cl-36	1(p)	$D1^2$ = 19200 D1=6600	5.87(80) 17.6(23)	6.9/0.9	16.2(19) 48.6(58)	6.3/0.3
	s(th)	Do=22300	1.25(10)	6.3/0.3	0.32(1)	6.5(0.5)
Cl-38	s(th)	na				
Sc-46	2(s)	Do=1030	0.46(10)	7??	0.63(20)	7.2??
	s(th)	Do=1030	3.66(40)	6.5/05	3.03(40)	6.4/0.4
Ti-49	s(th)	Do=20800	10.44(105)	6.6/0.2		
V-51	s(th)	Do=1760	1.34(13)	6.5/0.5		
V-52	s(th)	Do=3950	11.60(120)	6.4/0.5		
Cr-51	s(th)	Do=1400	1.7(2)	6.2/0.2		
Cr-53	1(p)	$D1^{3/2}$=15750 D1 = 10500	5.44 (167) 8.16(150)	4.2/0.5	1.53(13)	6.3/1.6
Cr-54	8(s)	Do=7100	9.80(150)	6.9/2.8	0.59(7)	6.7/2.3
	15(p)	D1=2200	6.90(170)	5.9/0.8		
	s+p		8.35(160)	6.9/2.8		
Fe-57	1(p)	$D1^{1/2}$=23100 D1 = 8210	0.17(9) 0.49(16)	4.3/0.4	0.48(10)	5.5/2.2
	s(th)	Do=22000	1.28(20)	6.2/0.2		
Fe-58	s(th)	Do=7050	4.23(50)	6.5/0.5		
Fe-59	2(p)	D1=5030			0.45(15)	5.4/1.2
Co-60	1(s)	Do^4=3128 Do = 1390	2.45(60) 5.51(135)	6.9/0		
Ni-59	s(th)	Do=19920	1.27(10)	6.3/0.3		
Ni-61	s(th)	Do=14500	0.97(10)	6.4/0.4		
Ni-63	s(th)	Do=16400	5.36(34)	6.5/0.2		
Cu-63	4(s)	Do=700	2.72(68)	6.8/0.4	4.08(102)	6.3/0.1
	s(th)	Do=722	2.32(20)	6.5/0.5	0.25(3)	6.5/0.2
Cu-65	s(th)	Do=1520	3.60(10)	6.4/0.4		

Zn-65	s(th)	Do=2940	3.61(27)	6.5/0	0.47(3)	6.1/0
Zn-68	s(th)	Do=367	2.22(42)	6.5/0.4	0.77(11)	6.2/0.1
Ge-74	6(s)	Do=99	5.65(140)	7.1/0.6	2.17(55)	7.6/1.1
Nb-94	3(s)	Do=84.8			1.01(34)	6.6/0.6
	4(p)	D1=50	7.65(191)	6.6/0.6		
	s(th)	Do=95.6	3.70(30)	6.6/0.2	8.14(80)	6.5/0.5
Mo-93	7(s)	Do=2700			1.38(35)	6.4/0.7
	16(p)	D1=780	7.36 (220)	6.9/1.2		
Mo-99	6(s)	Do=970			0.44(11)	5.5/0.5
	11(p)	D1=286	6.28(159)	5.5/0.5		
Ru-100	4(s)	Do=21.3	8.48(212)	7.1/0.1	2.42(0.73)	7.2/0.4
	s(th)	Do=22			9.75(98)	6.5/0.5
Ru-102	6(s)	Do=18	21.7(54)	6.9/0.3	10.5(26)	7.1/0.5
	s(th)	Do=18.5	16.3(8)	6.0/0.5	17.9(8)	6.7/0.2
Rh-104	7(s)	Do=32	4.72(118)	6.7/0.3	1.31(39)	6.8/0.2
	s(th)	Do=26.8	5.2(4)	6.7/0.4	0.5(2)	6.6(0.2
Pd-106	9(s)	Do=10.9	3.87 (39)	7.0/0.4	0.91(28)	8.1/0.9
	s(th)	Do=10.9	4.77(30)	6.7/0.3	1.27(20)	6.8/0.2
In-116	23(s)	Do=9	11.9(30)	6.1/0.3	0.91(23)	6.1/0.2
Sb-122	12(s)	Do=10	12.3(31)	6.3/0.5	1.64(46)	6.3/0.5
Sb-124	4(s)	Do=24	4.79(126)	6.2/0.2	0.8(2)	6.3/0.2
Te-126	6(s)	Do=42.7	6.83(167)	5.9/0.4	1.32(46)	5.9/0.5
I-128	8(s)	Do=9.7	8.54(256)	6.6/0.2	1.08(38)	6.6/0.3
	s(th)	Do=9.7	9.79(41)	6.5/0.4	1.91(40)	6.5/0.5
Cs-134	s(th)	Do=20	3.41(20)	6.5/0.5	1.29(10)	6.5/0.5
Ba-136	10(s)	Do=40	6.17(123)	6.6	1.10(38)	7.0/0.3
Nd-144	10(s)	Do=37.6	6.17(117)	6.4/0.7		
Nd-146	na	Do=17.8	4.50(18)	6.7		
Sm-148	23(s)	Do=5.7	4.39(117)	6.3/0.7	1.39(35)	5.3/0.3
Sm-150	3(s)	Do=2.2	5.42 (136)	6.5/0.7		
Eu-154	s(th)	Do=1.14	10.0(62)	6.5/0.2	0.96(2)	6.6/0
Gd-153	na	Do=13.5	11.0(3)	na		
Gd-155	na	Do=13.8	8.70(18)	5.9		
Gd-157	na	Do=30.5	12.4(223)	6		
Gd-159	12(s)	Do=87	9.21(230)	5.2/0.7	1.22(32)	5.1/0.3
Er-168	81(s)	Do=4	16.6(325)	6.4/0.3	4.23(102)	6.4/0.3

Er-169	4(s)	Do=94	7.31(119)	5.3/0.7		
Tm-170	10(s)	Do=7.28	6.31(126)	6.1/0.5	1.42(43)	6.0/0.2
Lu-176	12(s)	Do=3.45	4.57(62)	5.8/0.2		
Lu-177	6(s)	$Do^{15/2}$=3.03	43.9(21)	6.3/0.3		
	6(s)	Do=1.61	23.3(11)	6.3/0.3		
	s(th)	Do=1.61	24.06(248)	6.4/0.4	9.87(149)	6.4/0.4
Y-174	24(s)	Do=8.06	37.8(67)	5.7/0.2		
	s(th)	Do=8.06	23.0(19)	5.7/0.2	1.39(27)	6.0/0.1
Hf-178	20(s)	Do=2.32	31.7(676)	6.0/0.3	4.62(88)	6.0/0.3
	s(th)	Do=2.32	35.7(54)?	6.2/0.3	11.7(18)	6.0/0.3
Ta-182	19(s)	Do=4.4	9.2(19)	5.6/0.4	1.3(3)	5.6/0.4
W-183	7(s)	Do=63.4	10.6(26)	5.6/0.6		
W-184	6(s)	Do=12	36.9(99)	6.5/0.9		
	s(th)	Do=13.7	53.3(27)	6.2/0.3		
Pt-196	22(s)	Do=16.3	17.2(22)			
Au-198	4(s)	Do=15.7	20.0(41)	6.2/0.3		
Hg-199	2(s)	Do=105	27.8(30)	6.3/0.3	1.3(6)	5.6/0.3
Hg-200	3(s)	Do=85	14.3(209)	7.0/1.0		
Hg-202	3(s)	Do=90	33.7(80)	7.0/0.7		
Th-233	5(s)	Do=15.82	30.0(82)	4.0/0.3	8.33(212)	4.2/0.3
	s(th)	Do=15.82	12.2(12)	4.0/0.2	8.1(9)	4.1/0.1
U-235	3(s)	Do=12.3	9.8(19)	4.4/0.3	2.46(11)	4.4/0.3
U-236	19(s)	Do=0.49	7.14(131)	5.8/0.6		
U-237	7(s)	Do=14.7	4.45(112)	4.4/0.2	0.23(6)	4.6/0.5
U-239	23(s)	Do=16.4	7.70(173)	3.8/0.3	2.10(57)	4.2/0.6
Pu-240	7(s)	Do^{1} = 2.73	18.0(48)	5.8/0.7	2.68(67)	6.1/0.4
	7(s)	Do = 2.07	23.7(63)			

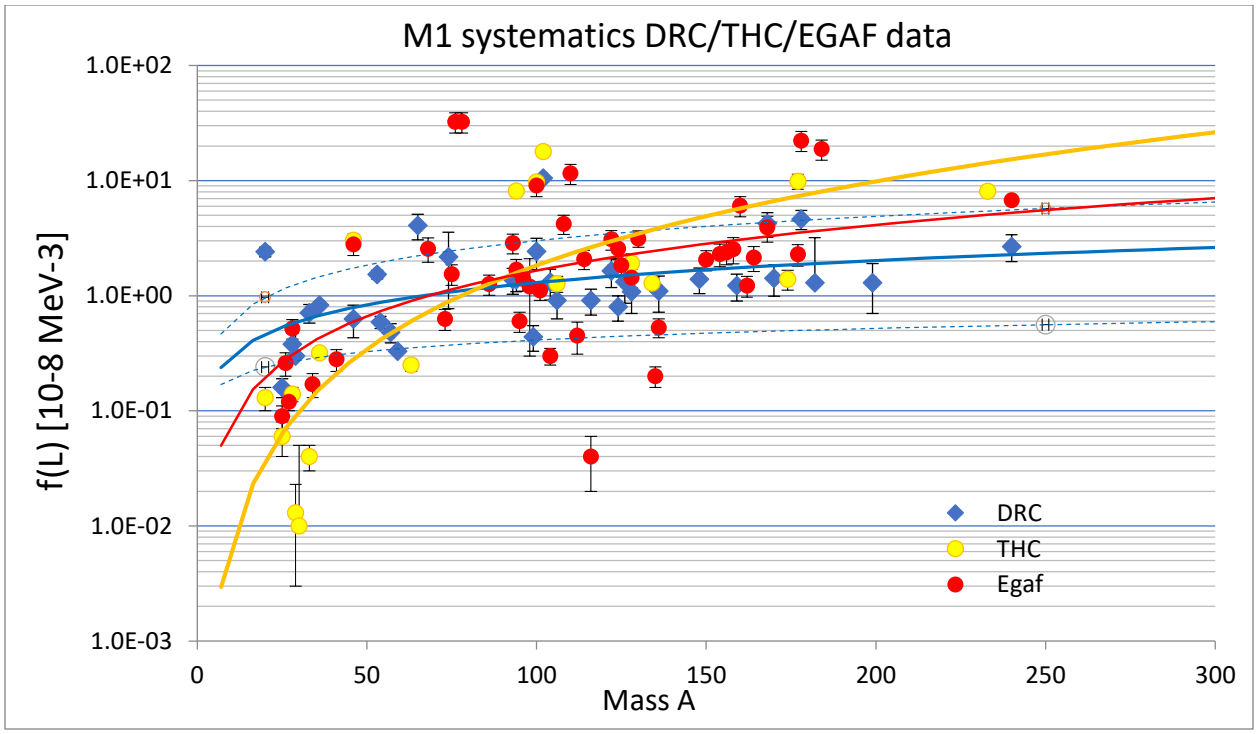

Fig.25 *Quasi-mono energetic doubly average strength functions <<f(M1)>> from recent evaluations using DRC (blue diamonds) [4] and THC (yellow circles) data [8] and EGAF (red points) [10]. The fitted trend curves are power mass A dependent. The dotted line is one SD dispersion from the LSQ procedure of the DRC data.*

It is interesting to compare the difference in the data fluctuations between the E1 and M1 radiation. This comparison is graphically displayed in Fig. 26. The E1 data consistently follow similar trend-curves with relatively small fluctuations. However, for the M1 data the situation is different. The trend lines have a similar shape but with different absolute values and large data fluctuations, especially for the EGAF data. The reason could, as mentioned earlier, be found in the worse averaging but probably is also due to the structure of the M1 strength response deviating from a smooth dependence.

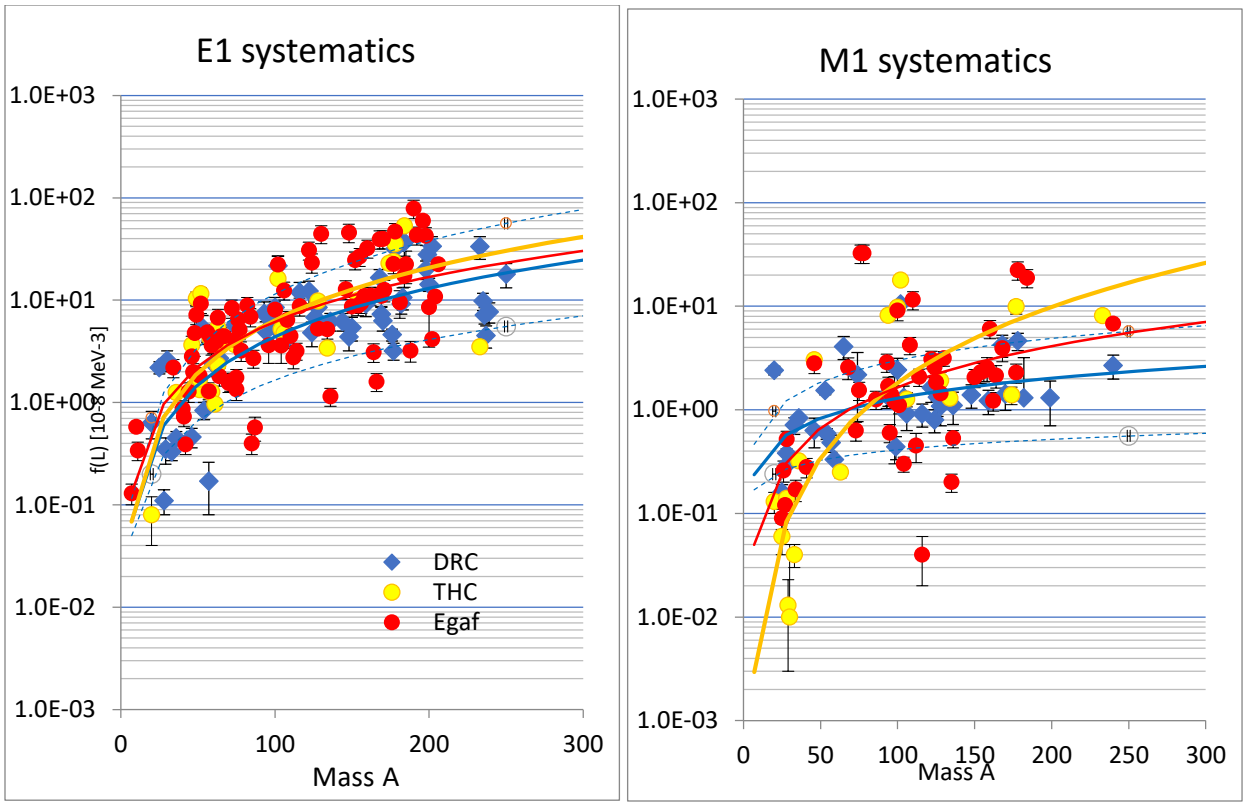

Fig.26 *Comparison of quasi-mono energetic strength <<f(E1)>> and <<f(M1)>> functions from recent evaluations of DRC (blue diamonds) [4] and thermal data from THC (yellow circles) data [8] and EGAF(red points) [10], respectively. The fitted trend curves are power laws of the mass A. The dotted lines are one SD dispersion from the LSQ method of the DRC data (for details see [4]). Note much larger fluctuations of the M1 data.*

4. Generalized E1 and M1 slope analysis

The $E\gamma^L$ reduction exponent L has been proposed in Ref. [8] as an adjustable parameter, which gives an information about the reaction mode. It represents an estimate of the Eγ dependence of the data slope from unweighted trend curves in an energy region chosen from the data. This is described in detail in Ref. [7] and illustrated in Fig. 10 of that reference. This is demonstrated for the PSF data from the ^{45}Sc(n,γ) reaction, shown in Fig. 10, with fitted trend lines in the E_γ^3 power format. At this point we need to bear in mind, that the PSF is defined in the Eγ-dipole space factor E_γ^3 format and the trend reduction exponent L can be calculated from the following relationship

$$L(\text{trend}) = L(\text{theory}) - 3 \qquad (4).$$

For example, the compound nucleus predicts L(trend) = 5 – 3 = 2. The accuracy of the Eγ-dependence of I_γ/E_γ^L is strongly related to the number of data points but mainly to the sample size, given by the broadness of the energy region of the data. The unweighted trend derivation can be strongly influenced by one or two extremely deviating data points. However, if enough nuclides are involved, a general conclusion on the L trend can certainly be achieved. The L values of the reduced intensities I_γ/E_γ^L extracted from the THC data are listed in Table 5. It should be noted that only the THC data allow an analysis to be made of the PSF slope.

A detailed discussion of light nuclides with A < 70 can be found in Ref. [8]. In this section we extended this study by the addition of several entries for heavier nuclides and this opens a possibility to draw conclusions for data up to A ~ 250. Their number is not large, but still gives a reasonable insight to the general behavior of L-values for heavier nuclides.

Table 5 The list of relevant slope values needed for qualification of the presence of nonstatistical or statistical processes. Entries for L and $<E\gamma^L>$ given in red, the entry gets a warning, either where there are too small numbers of PSF data points or a too narrow (< 1 MeV) energy region.

$<L>_{trend}$ - the average E_γ exponent derived from the trend fit of PSF data
$<L>_{theory}$ - n(max) the real E_γ^n dependence of the gamma-ray strength decay

Target	$E\gamma^{min}$–$E\gamma^{max}$	$<L>_{trend}$	$<E\gamma^L>$	$E\gamma^{min}$-$E\gamma^{max}$	$<L>_{trend}$	$<E\gamma^L>$
	<MeV>	PSF	$<L>_{theory}$	< MeV>	PSF	$<L>_{theory}$
	E1	E1	E1	M1	M1	M1
F-19	0.6 – 5.6	-4.17	-1.17	0.3 – 6.6	-1.80	1.2
Na-23	1.6 – 3.6	-0.82	2.18	0.7-6.5	-2.80	0.2
Mg-24	0.9 – 3.9	-0.39	2.61	2.2 – 6.7	-2.31	0.69
Mg-25				4.0 – 11.0	-1.35	1.65
Al-27	1.9 – 4.3	-1.67	1.33	0.4 – 7.8	-3.08	-0.08
Si-28				1.6 – 8.5	-2.09	0.91

Si-29				4.0 – 10.6	-3.19	-0.19
P-31	1.7 – 4.7	-0.91	2.09	1.1 – 7.9	-2.78	0.22
S-32	2.1 – 5.4	-0.64	2.36	2.0 – 8.6	-2.16	0.84
Cl-35	1.9 – 6.6	-1.60	1.40	2.0 – 8.6	-1.21	1.79
Cl-37	1.3 – 6.1	-1.01	1.99			
K-39	2.3 – 7.8	-0.76	2.24	3.9 – 5.5	-2.46	0.54
Ca-40	3.6 – 6.4	-0.60	2.40	3.4 – 6.4	-4.18	-1.14
Sc-45	4.6 – 8.8	-1.48	1.52	5.3 – 8.5	0.29	2.71
Ti-48	2.3 – 6.8	1.79	4.79	2.7 – 8.6	-1.98	1.02
V-50	4.1 – 9.4	0.10	3.1	2.3 – 5.6	-1.36	1.64
V-51	3.5 – 7.3	2.45	5.45			
Cr-50	5.2 – 8.5	2.67	5.67			
Fe-56	2.4 – 7.6	1.56	4.56	2.4 – 5.3	-1.96	1.04
Fe-57	4.6 – 10.0	-2.51	0.49			
Co-59	3.9 – 7.5	0.84	3.84	2.7 – 5.1	-4.68	-1.68
Ni-58	3.9 – 9.0	1.50	4.50			
Ni-60	3.4 – 7.8	4.14	7.14	3.6 – 7.2	-5.35	-2.35
Ni-62	2.4 – 6.8	1.34	4.34	3.1 – 3.6	-0.27	2.73
Cu-63	3.6 – 7.9	-0.21	2.79	3.5 – 6.6	-3.75	-0.75
Cu-65	3.6 – 7.1	-1.83	1.17	2.5 – 4.9	-2.29	0.71
Zn-64	4.8 – 7.9	1.81	3.1	3.6 – 6.1	-4.15	-1.15
Zn-67				4.9 – 7.5	-6.57	-3.57
Nb-93	5.9 – 6.8	6.3	9.23	4.9 – 7.2	-2.0	1.0
Ru-99				6.2 – 9.7	-7.9	-4.9
Ru-101				6.2 – 8.7	-6.2	-3.2
Rh-103	5.7 – 7.0	-4.0	-1.0	5.2- 6.9	-4.6	-1.6
Pd-105				6.7 – 9.0	-3.7	-0.7
I-127	5.1 – 6.7	1.6	4.6	4.6 – 6.8	-7.3	-4.3
Cs-133	5.6 – 6.6	-5.1	-2.1	5.9 – 7.0	-2.4	0.6
Ba-135				5.1 – 9.1	-2.8	0.2
Ba-137				4.0 – 8.6	-5.5	-2.5
Nd-146	4.6 – 7.1	7.0	10.0	4.7 – 6.4	-2.7	0.3
Eu-154						
Yb-173	4.6 -7.4	0.3	3.3	5.6 – 6.2	-10.2	-7.2
Lu-176	5.7 – 6.4	8.9	11.2	5.7 – 6.7	-0.2	2.8
W-183	4.4 – 7.4	2.3	5.3	(5.2 – 6.3)	(1.23)	
Th-232				3.7 – 4.2	-8.85	-5.85

The L-slope results for E1 transitions are shown in Fig. 27. The GRM has been widely accepted as a model which governs the E1 strength distribution below the neutron binding energy B_n and has been verified theoretically and experimentally for data in the E_γ region of several MeV below B_n. The present analysis is often, especially for light nuclides, extended to low gamma ray energies and shows a deviation of the GRM predicted shape. The fitted slope behavior demonstrates an increase of the E1 strength with E_γ -> 0, the feature which was in Ref. [8] accounted for by the

presence of nonstatistical direct and valence capture components. The step of L values from the negative to positive numbers is shown in detail in the figure by data for A < 70. This is certainly only a qualitative conclusion, owing to large uncertainties of the L derivations, but the trend and the mean L values are convincing.

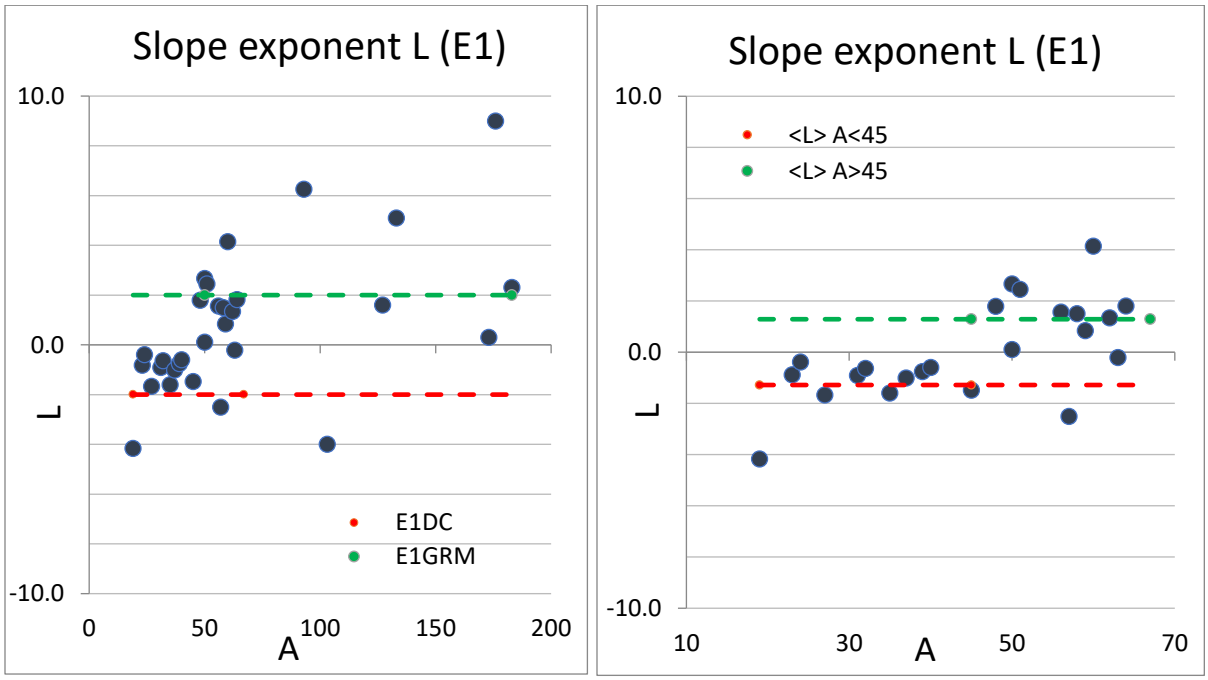

Fig.27 *Values of <L> derived from the "slope" analysis of the E1 PSF data. Note the expected negative values for targets with A < 50 (dominating nonstatistical mode) to and A > 50 data with the statistical GR model. This is shown in detail in the righthand part of the figure (discussed in detail in Ref. [7]). The outliers are due to a very narrow E_γ window of E1 transitions (see red entries in Table 5). The green and red lines in the left figure show the expected L values from the Direct Capture (red) and the E1GR (green) models. The right figure shows the mean L values for A ≤ 45 nuclides as ~ $E_\gamma^{-1.28}$ and for A > 45 ~ $E_\gamma^{1.29}$ which gives for underlying models satisfactory values of $E_\gamma^{1.8}$ (DCM) and $E_\gamma^{4.29}$(GRM), respectively.*

The M1 transitions show a consistent decrease of negative L values with increasing mass A, as shown in Fig. 28. The data dispersion is relatively small which supports the general conclusion that the M1 strength below the spin-flip resonance has an increasing trend in the whole mass region. However, the absence of sufficient data above A~150 increases the uncertainty of the derived trend equation

$$<L> = – 0.024A – 1.68,$$

that the shape is steeper with the increasing A. This rather crude qualitative conclusion needs to be tested by theoretical modelling. The proposed combination of the M1 strength below Bn from

the spin-flip, the scissors and up-bend modes form the adopted models of excitations and their absolute strength is to be explained, at least for the discussed neutron capture THC results.

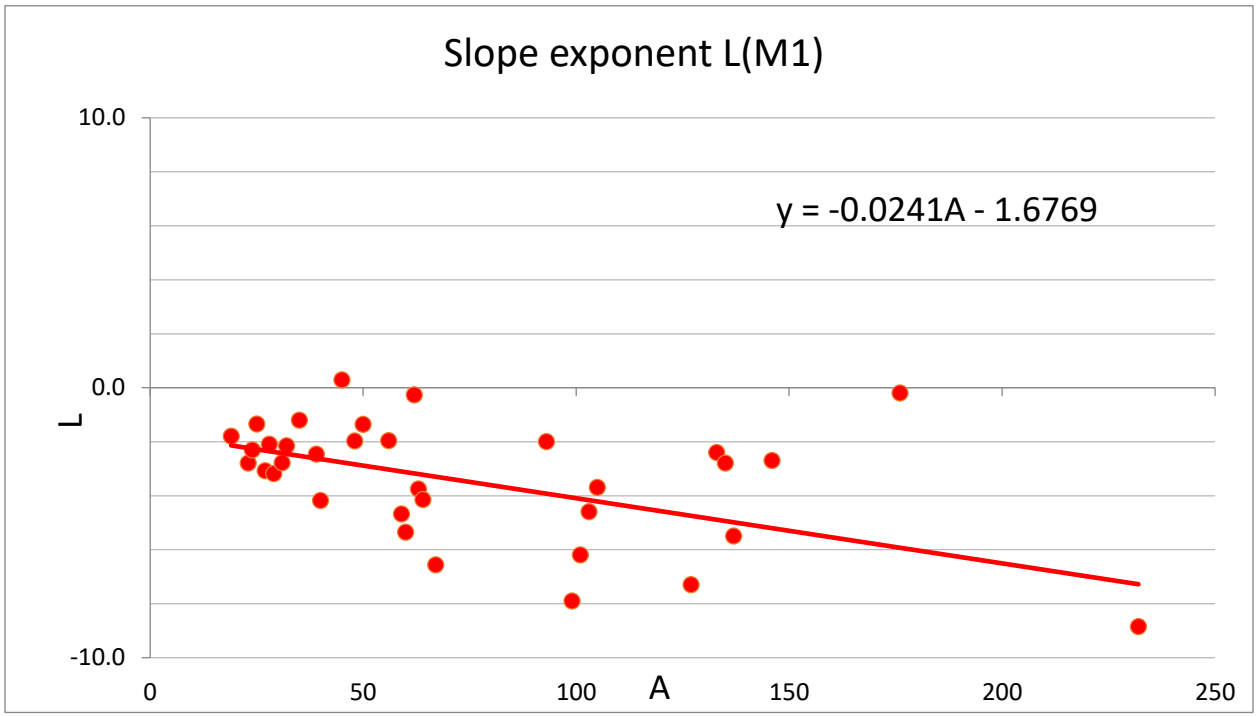

Fig.28 *Values of <L> derived from the "slope" analysis of the M1 PSF data. Note a rather systematically decreasing trend of negative L values for A -> 250 with a limited number of outlier (only one strongly deviating point at A = 176).*

One of the reasons for the sharp decrease of the L-value with the mass A could be due to increasing lower energy of the ΔE_γ window for heavier nuclides. This feature, experimentally understood, can influence the steepness of the data trend from a narrow fitting region and also probably from a larger contribution from the spin-flip resonance. Another view of this situation is given in Fig. 29 where the ΔE_γ window width is plotted as an error bar of mean $<E_\gamma>$ values (red points) for fitted L values. Two groups of data points exist, one around L~ -2 with $<E_\gamma>$ ~ 2.5 MeV (light nuclides) and heavier nuclides with $<E_\gamma>$ ~ 5 MeV with L-values between -4 and -6. More THC evaluations for heavier nuclides with A > 150 may give more input and help to improve the accuracy of the L values behavior in this mass region.

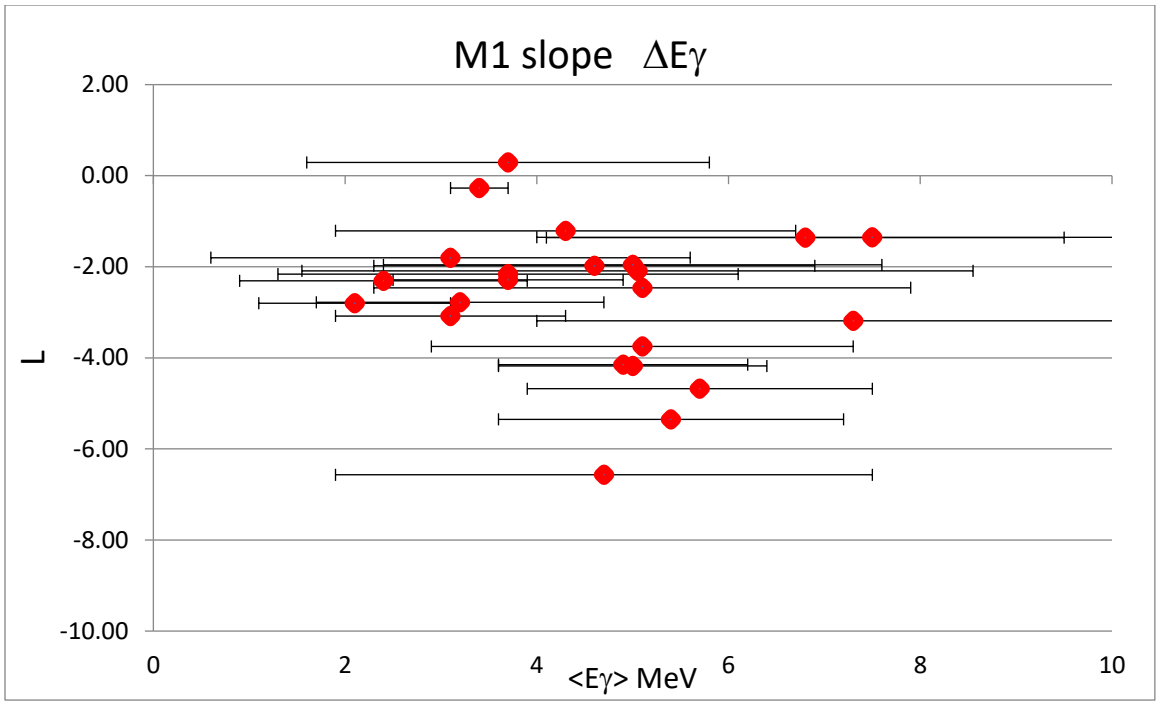

Fig.28 *Values of <L> derived from the "slope" analysis of the M1 PSF data as a function of the mean <E_γ> energy (red points) and the size of the energy window ΔE_γ shown as horizontal error bars. The order of the mass goes vertically down through the plotted points. Note the shift of L-values upwards with the mass and widths of the window.*

5. Comparison of experimental data with D1M+QRPA

The final THC and DRC library of PSF is now compared with the prediction of the so-called D1M+QRPA+0lim model. All details of the model can be found in Ref. [7] (and references therein). Such QRPA calculations based on the Gogny D1M interaction include some phenomenological corrections that have been adjusted to experimental data [7]. These include a broadening of the QRPA strength to take the neglected damping of collective motions into account as well as a shift of the strength to lower energies due to the contribution beyond the 1 particle - 1 hole excitations and the interaction between the single-particle and low-lying collective phonon degrees of freedom. When considering the deexcitation PSF, deviations from the photo-absorption strength are expected, especially for γ-ray energies approaching the zero limit. For this reason, a low-energy constant E1 strength and an M1 upbend, both inspired by shell-model calculations, were added to the D1M+QRPA strength and adjusted to existing data. The E1 and M1 PSF, including the low-energy contributions is referred to as D1M+QRPA+0lim.

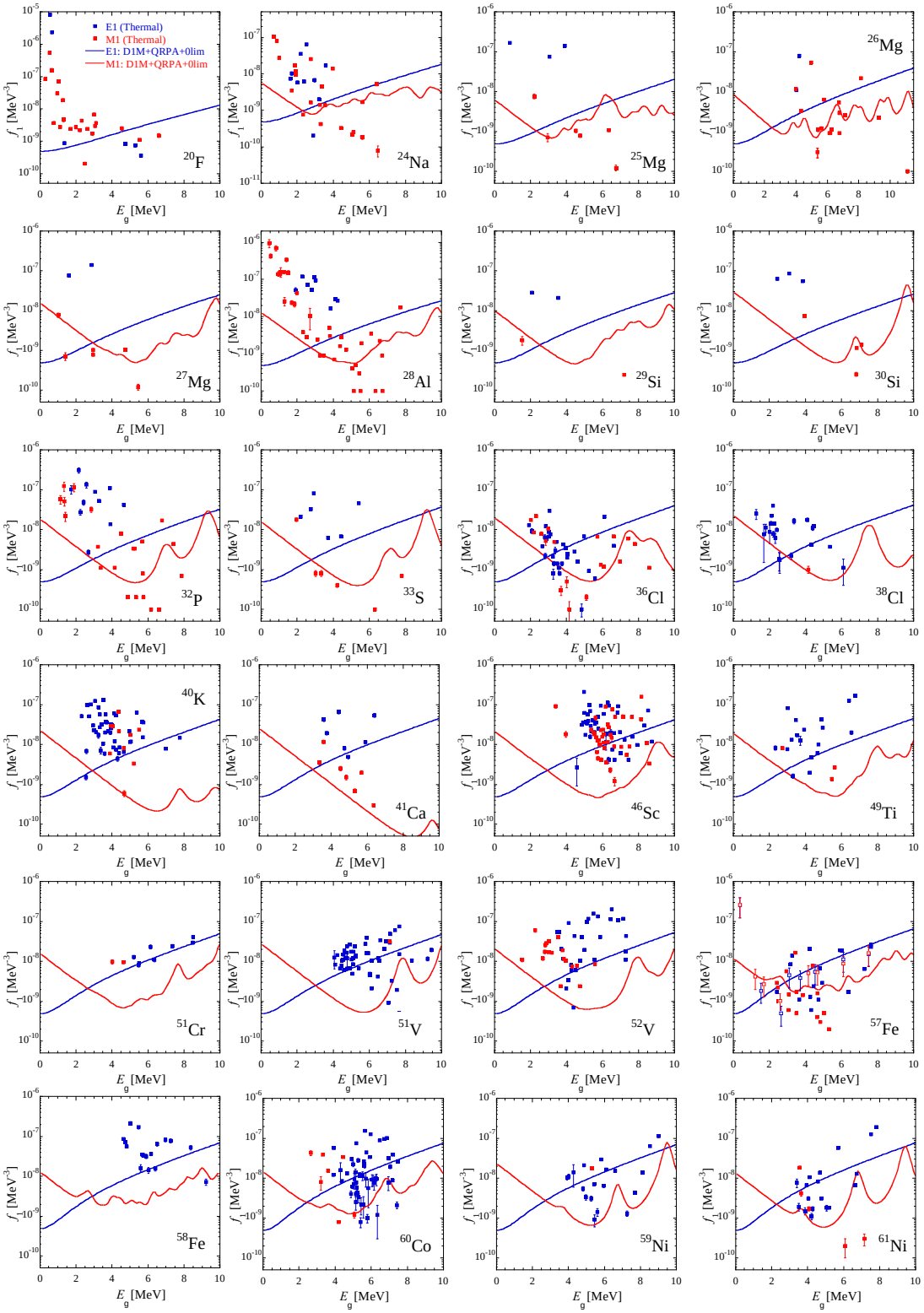
E1 (Thermal)
M1 (Thermal)
E1: D1M+QRPA+0lim
M1: D1M+QRPA+0lim
f_1 [MeV^{-3}]
E_g [MeV]
^{20}F
^{24}Na
^{25}Mg
^{26}Mg
^{27}Mg
^{28}Al
^{29}Si
^{30}Si
^{32}P
^{33}S
^{36}Cl
^{38}Cl
^{40}K
^{41}Ca
^{46}Sc
^{49}Ti
^{51}Cr
^{51}V
^{52}V
^{57}Fe
^{58}Fe
^{60}Co
^{59}Ni
^{61}Ni

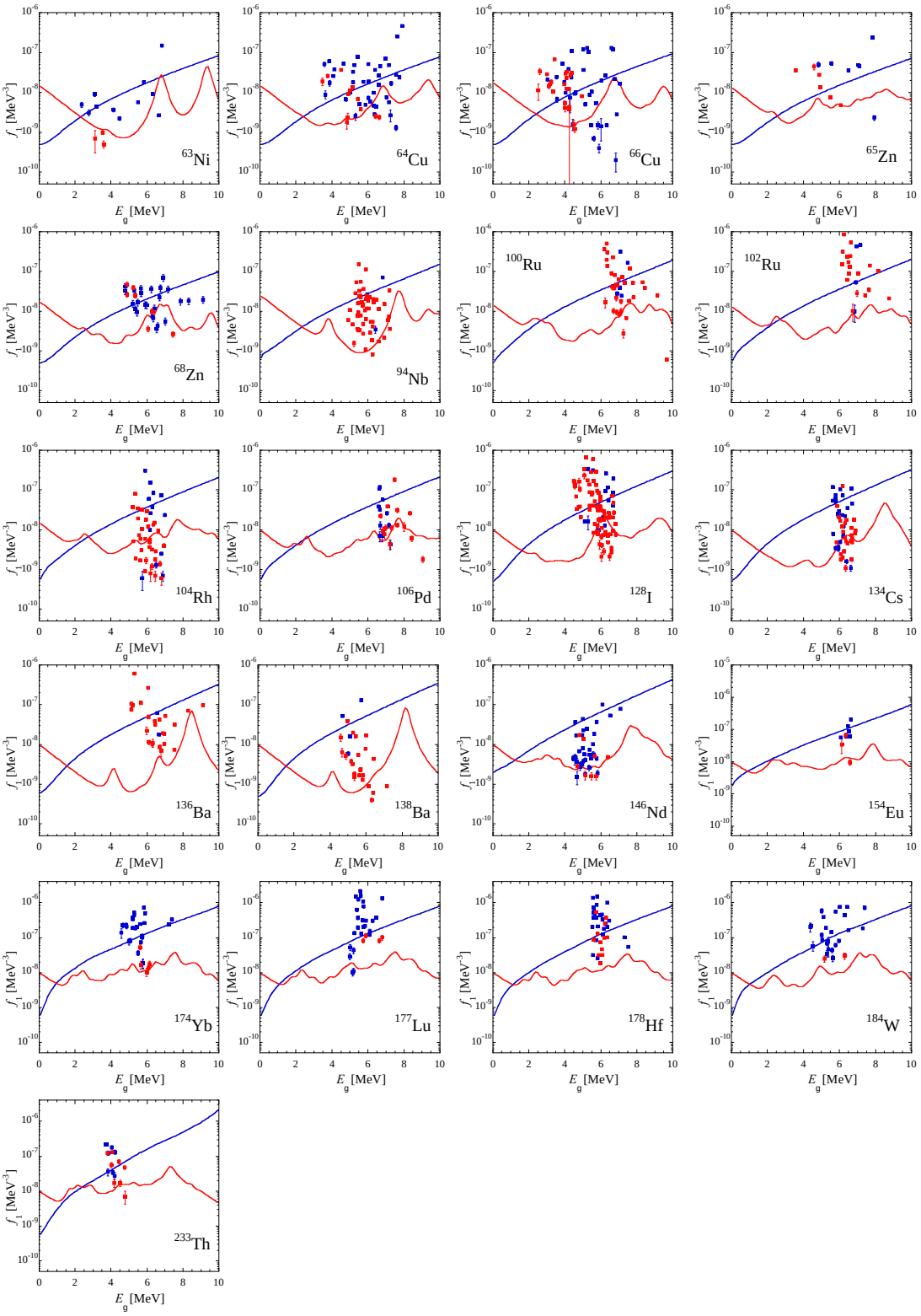

Fig.29 *Comparison between the E1 (blue) and M1 (red) PSF extracted from all THC data (squares) with the D1M+QRPA+0lim model (solid lines)*

The E1 and M1 PSF extracted from the THC data for 45 nuclei are compared with the D1M+QRPA+0lim model in Fig. 29. The THC data have the peculiarity to extend to rather low energies reaching values down to 1-2 MeV, especially for light nuclei. THC data clearly show the low-energy M1 upbend which has originally been inferred from the Oslo data [7]. The phenomenological upbend introduced in the D1M+QRPA+0lim model is seen to reproduce rather fairly the data, although quantitatively significantly more strength is found in ^{24}Na, ^{28}Al or ^{32}P THC data. However, the extraction of the PSF for these nuclei remains affected by the contribution of nonstatistical processes that remain difficult to evaluate as discussed previously [8]. Concerning the E1 PSF, the agreement between theory and THC data is rather good, as already pointed out.

The E1 and M1 PSF extracted from the DRC data for 52 nuclei are compared with the D1M+QRPA+0lim model in Fig. 30. In most of the cases, the DRC PSF are rather well reproduced by the QRPA model, especially for medium and heavy mass nuclei. For some specific light nuclei, like ^{36}Cl , ^{53}Cr, the experimental strength is underestimated. In contrast to THC data, the PSF from DRC is restricted to energies above typically 4 MeV, so that DRC data can hardly confirm the presence of an M1 upbend.

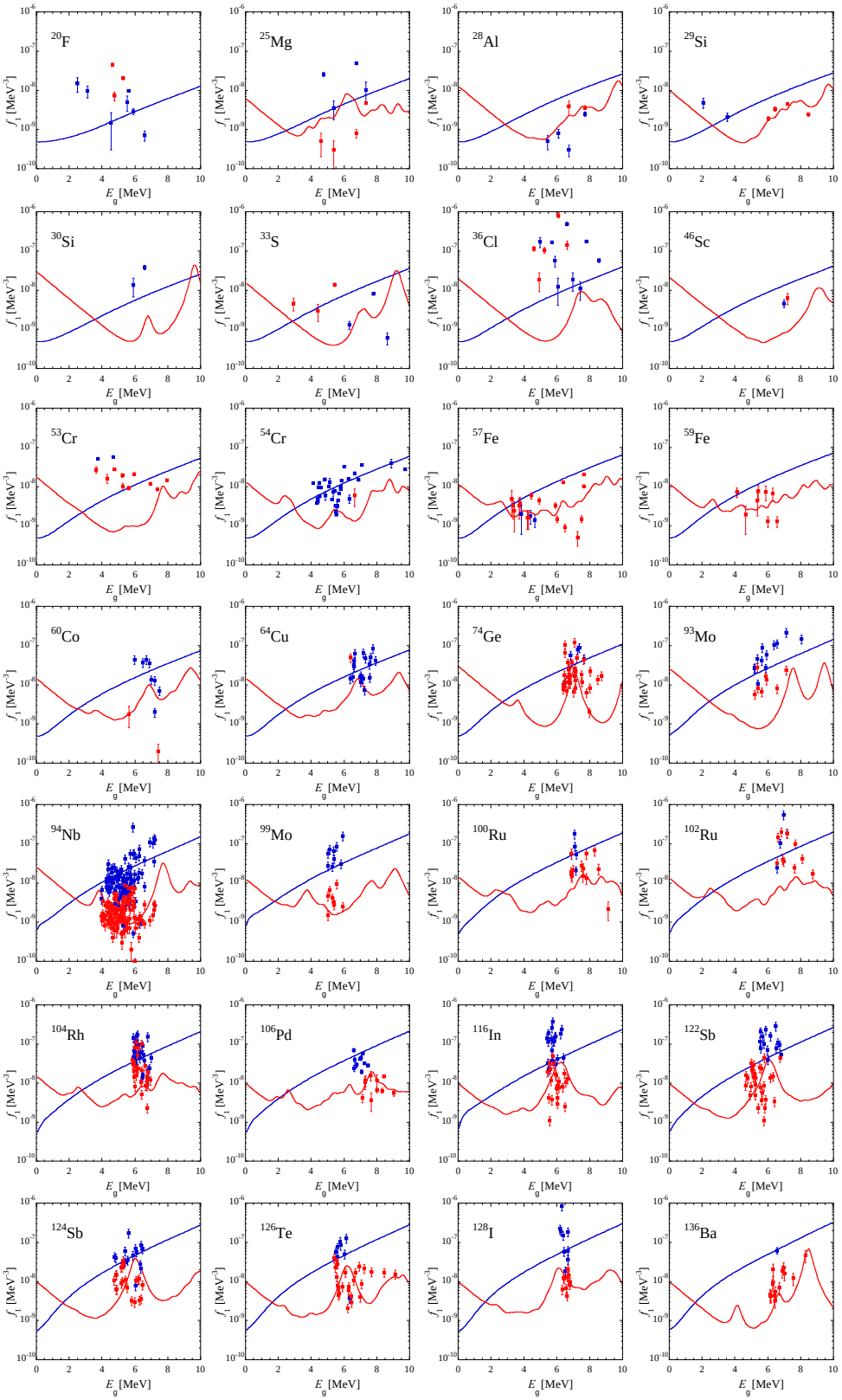
^{20}F
^{25}Mg
^{28}Al
^{29}Si
^{30}Si
^{33}S
^{36}Cl
^{46}Sc
^{53}Cr
^{54}Cr
^{57}Fe
^{59}Fe
^{60}Co
^{64}Cu
^{74}Ge
^{93}Mo
^{94}Nb
^{99}Mo
^{100}Ru
^{102}Ru
^{104}Rh
^{106}Pd
^{116}In
^{122}Sb
^{124}Sb
^{126}Te
^{128}I
^{136}Ba
f_1 [MeV^{-3}]
E_g [MeV]

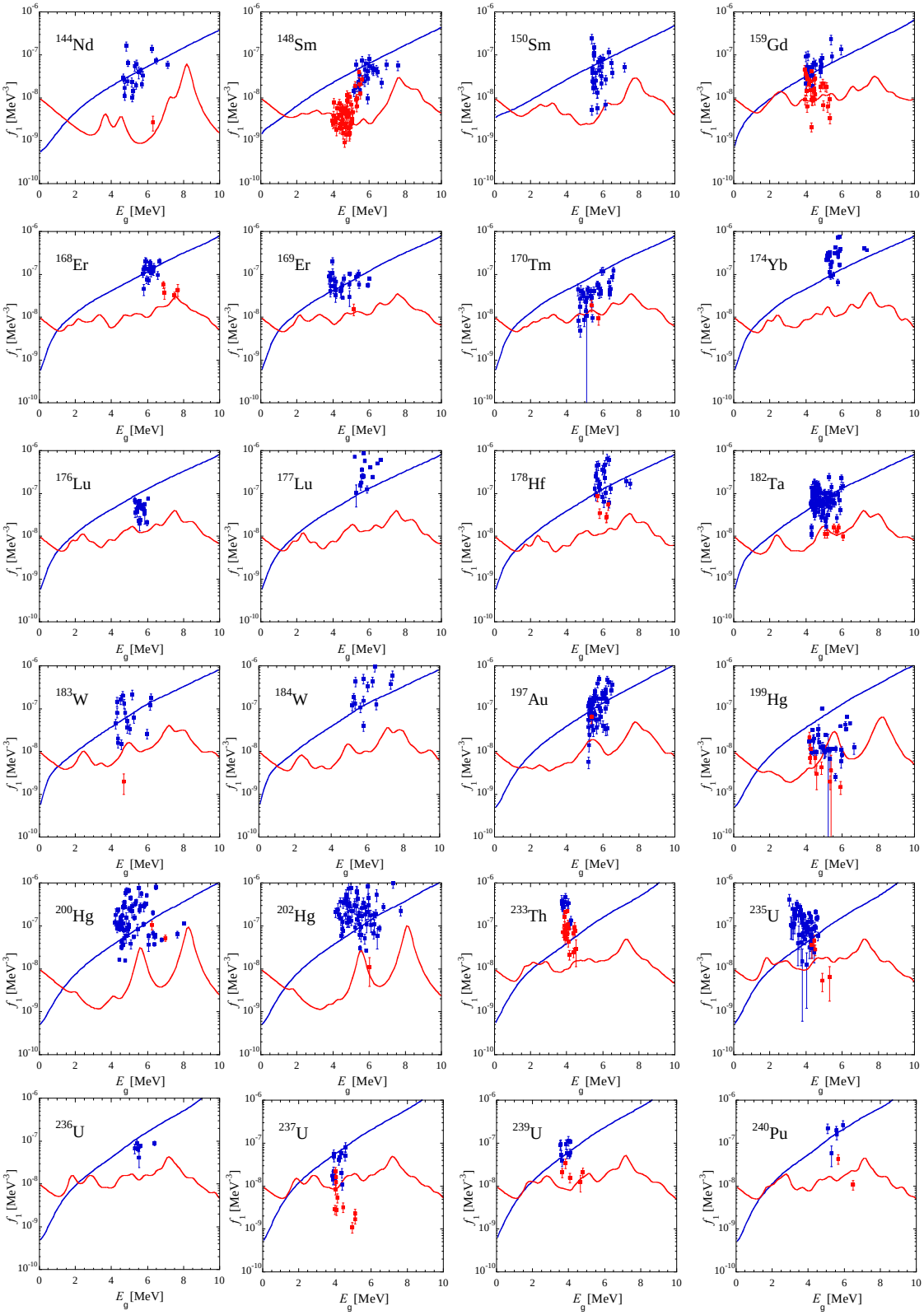

Fig.30 *Comparison between the E1 (blue) and M1 (red) PSF extracted from all DRC data (squares) with the D1M+QRPA+0lim model (solid lines)*

Summary

Recently a new interest in photonuclear data and consequently the associated gamma-ray strength functions has been initiated by the IAEA NDS organizing the start-up preparatory experts meeting at NDS [13]. This meeting opened the planned CRP on "*Updating Photonuclear Data Library and Generating a Reference Database for Photon Strength Functions"* scheduled for the period 2016 – 2018. One of the authors (JK) attended this meeting as an invited observer and when he realized that the subject of PSF from the neutron capture (a field in the first half of his career) was a relevant part of the study, he volunteered to work in this area with great support from Viviane Demetriou and Stephane Goriely.

This involvement, continuously supported by VD and SG, resulted in a comprehensive collection of gamma-ray photon strength functions (PSF) papers [1-8] including the re-opening and re-analysis of earlier data, with the aim of completeness, for all the available THC, DRC and ARC data sources. Another objective of this work was to process the data and evaluate the results in a consistent manner, with one set of tools and comment on the possible reaction models involved.

Overviewing the whole collection of results and conclusions, we have realized that a number of additions and corrections of inaccuracies/errors should be made and these form the content of this "Addendum". Reading it, however, requires a detailed familiarity with the earlier reports.

Several new THC evaluations discussed in Chapter 2 and their graphical representation is given in the Appendix. The main contribution of Chapter 3 is a thorough revision of data and the derivation of the of quasi-mono energetic strength <<f(E1)>> and <<f(M1)>> at the mean energy $\langle E_\gamma \rangle \sim 6.5$ MeV. These systematics forms an important absolute calibration tool of the PSF values extracted from the DRC data, the only data set with uniquely defined initial states in contrast to the THC or ARC experiments. The earlier excellent agreement of E1 systematics with the theory is confirmed, while the situation with the M1 data opens questions to confront with the theoretical predictions.

The importance of the nonstatistical processes, especially for the light nuclides, have been recognized and discussed in Ref. [8]. Chapter 4 continues in this investigation using the semi-quantitative "slope" parameter to identify the presence of these processes compared with the statistical model for E1 transitions and bringing more information on the E_γ dependence of M1 P

In Chapter 5, theory is compared with the final updated PSF extracted from THC and DRC data for 45 and 52 nuclei, respectively. Both the E1 and M1 PSF are compared with the predictions from the D1M+QRPA+0lim model [7]. In general, the present PSF THC data confirm the low-energy M1 enhancement, also referred to as the M1 upbend. The experimentally PSF is generally well reproduced by theory.

Acknowledgments

My (JK) thanks go to Stephane Goriely, who supported the idea to look further at the thermal neutron capture data for PSF applications and providing all of the D1M+QRPA plots and to becoming a co-author of this report. Further thanks go to Arjan Koning and the IAEA NDS as the supporting institution initiating the whole action. I also acknowledge the long and important support of Viviane Demetriou, which also helped JK to participate in this project.

Finally, two more personal acknowledgments, to Robin Forrest for our continuing contact, both in the professional and the friendship sphere and to Lidija Vrapcenjak for friendly and patient help with all my requests on accessing ancient references.

References

[1] J. Kopecky, "*Present status of experimental gamma-ray strength functions derived from neutron capture*" INDC(NED)-013 (2016)

[2] J. Kopecky, "*Atlas of average resonance capture data (Starter file)*" INDC(NDS)-0738 (2017)

[3] J. Kopecky et al., Phys.Rev. C95 (2017) 054317

[4] J. Kopecky, "*Revisions and Updates of Experimental Gamma-ray Strength Functions derived from the Discrete Neutron Resonance Capture*" INDC(NDS)-0738 (2018)

[5] J. Kopecky and S. Goriely. "*Strength Functions derived from the Discrete and Average Resonance Capture"* INDC(NDS)-0790, July 2019

[6] J. Kopecky, "*Photon Strength Functions in Thermal Capture"* INDC(NDS)-0799 (2020)

[7] S. Goriely et al., "*Reference Database for Photon Strength Functions*", Eur. Phys. J. A (2019) 55

[8] J. Kopecky, "*Photon Strength Functions in Thermal Capture II"* INDC(NDS)-0815 (2020)

[9] S.F. Mughabghab "*Atlas of Neutron Resonances*" (Elsevier 2018)

[10] R. Firestone, private communication

[11] S. Goriely and V. Plujko, Phys.Rev. C99 (2019) 014303 and private communication

[12] R. E. Chrien et al., Phys.Rev. C3 (1971) 2054

[13] S. Goriely and P. Dimitriou, *Updating the Photonuclear Data Library and Generating a Reference Data Base for Photon Strength Functions,* INDC(NDS)-0712 (2016)

Appendix

Errata

Na-24 TH ECN Petten

Ig/100 captures extracted from T.A.A. Thielens et al., Nucl.Phys. A403 (1983) 13
<Ggo> = 0.81 eV mean value of 4 resonances Do = 122 keV
Sum Ig = 100 % based on imposed condition SumIgEg = 100Q
$\alpha = 0$

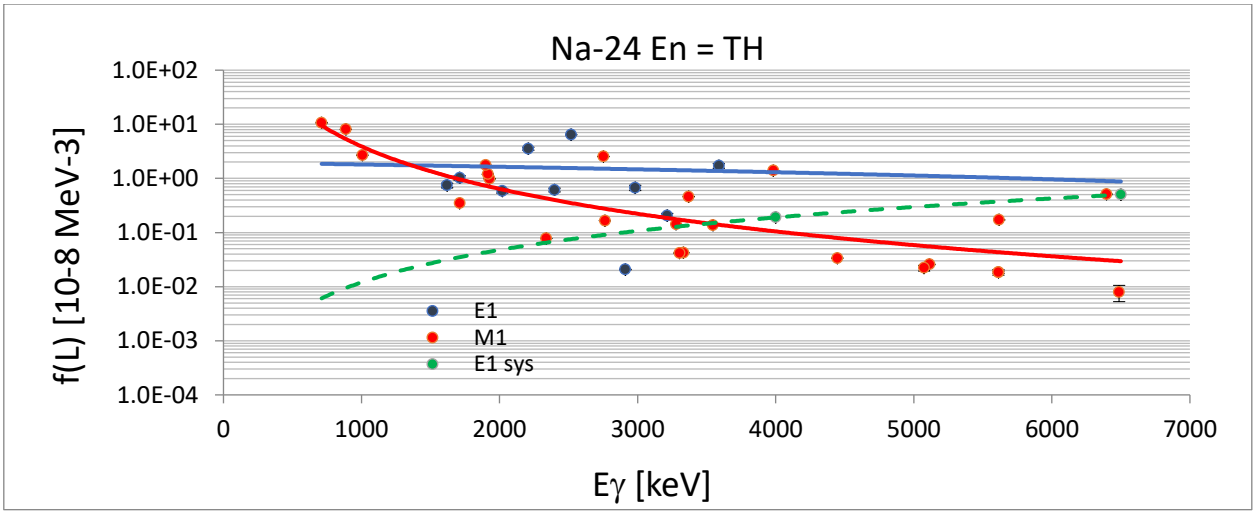

Cl-36 DRC BNL

Ig/100 captures extracted from R.E.Chrien and J. Kopecky Phys.Rev.Let. 19 (1977) 913
1 p-resonance 398 eV J = 2- Ggi = 0.46 eV
D1=6600 eV (D1(J=2) = 19200 eV not applied)
Porter-Thomas dispersion estimate: 1+dPT =√2/υ=2.4

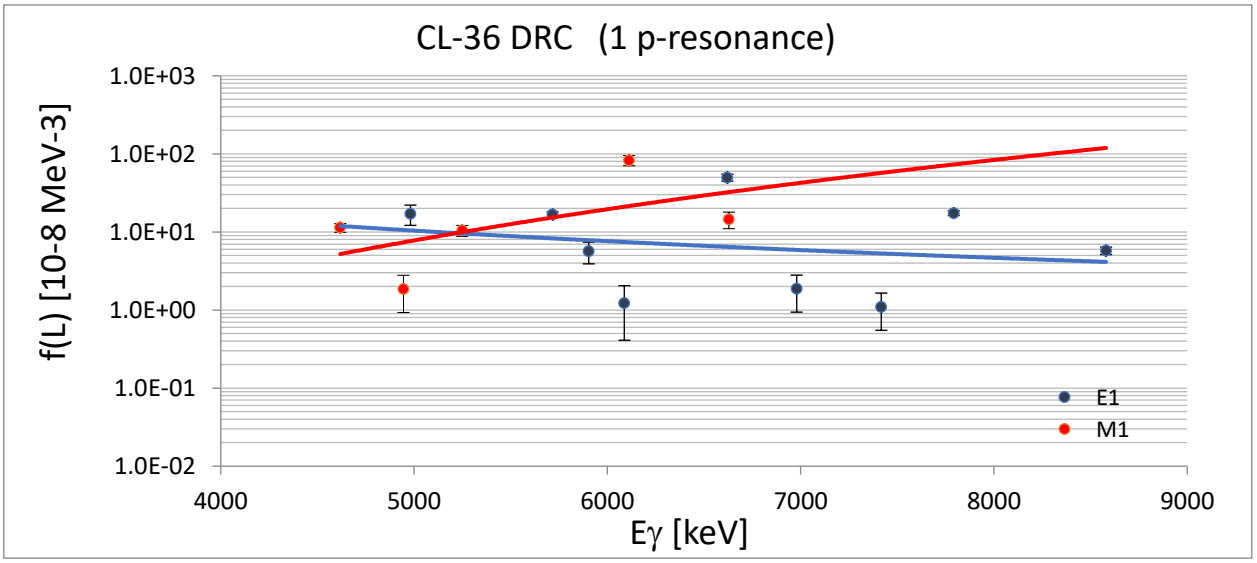

Cr-54 DRC Geel

Ggi for E1 from C. Coceva Il Nuovo Cimento Vol. 107 (1994) 85
<f(M1)> only given, no M1 individual transitions available in the data source
23 s-, p- resonances = 8 s- (J = 1-2-) and 15 p-wave (J = 1+2+3+) resonances
Porter-Thomas dispersion estimate: 1+dPT =√2/υ=1.28

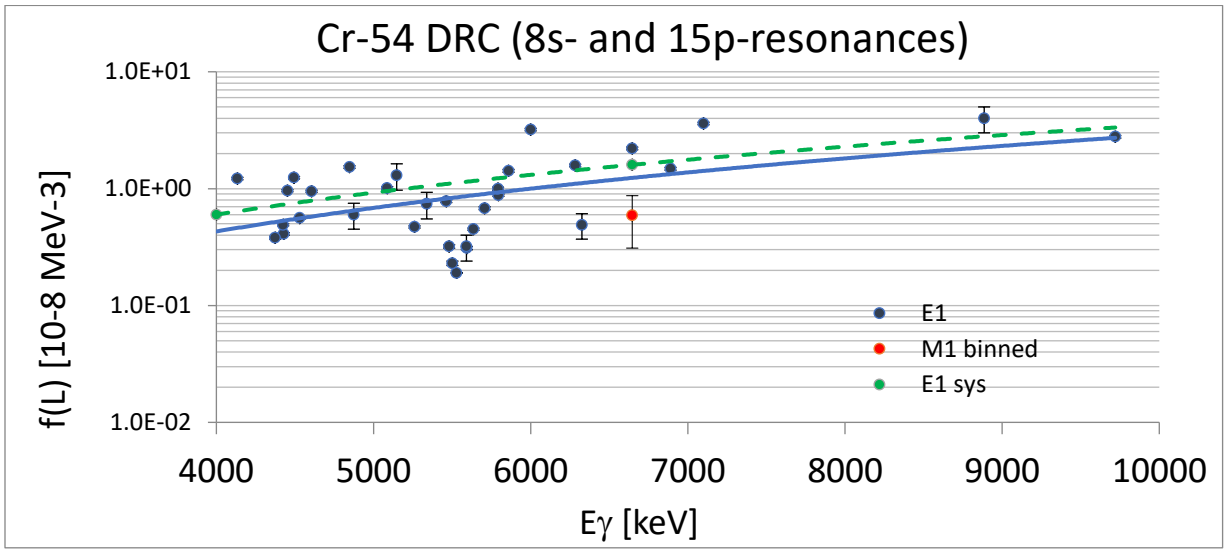

Fe-59 DRC Oak Ridge

Ig/100 neutrons extracted from J.C. Wells, Jr. et al. Phys.Rev. C18 (1978) 18
2 p-resonances = En = 230 eV and 359 ev J=?? <Ggi>p = 0.365 eV
D1 = 5030 eV
Porter-Thomas dispersion estimate: 1+dPT =√2/υ=2.0

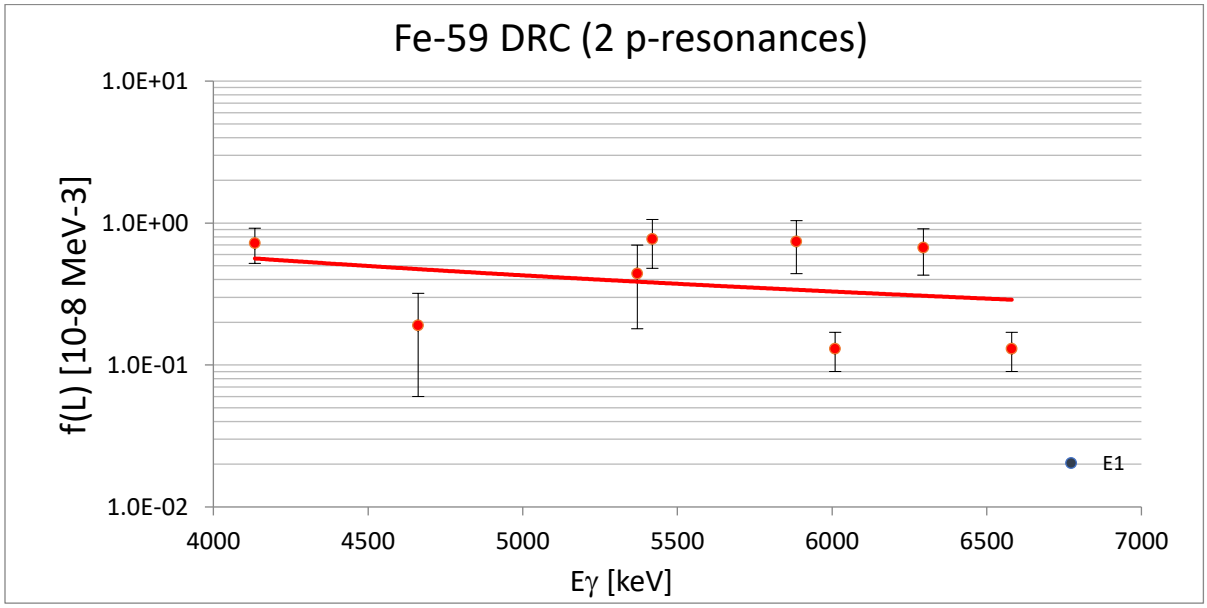

Lu-177 DRC Dubna

Ig/100 captures extracted from F. Becvar et al., Journal of Nuclear Physics (in Russian) 46(1987) 392
6 s-resonances = J=15/2- Ggo = 0.063 eV
Do= 1.61 eV //Do(J=15/2) = 3.03 eV not applied//
Porter-Thomas dispersion estimate: 1+dPT =√2/υ=1.57

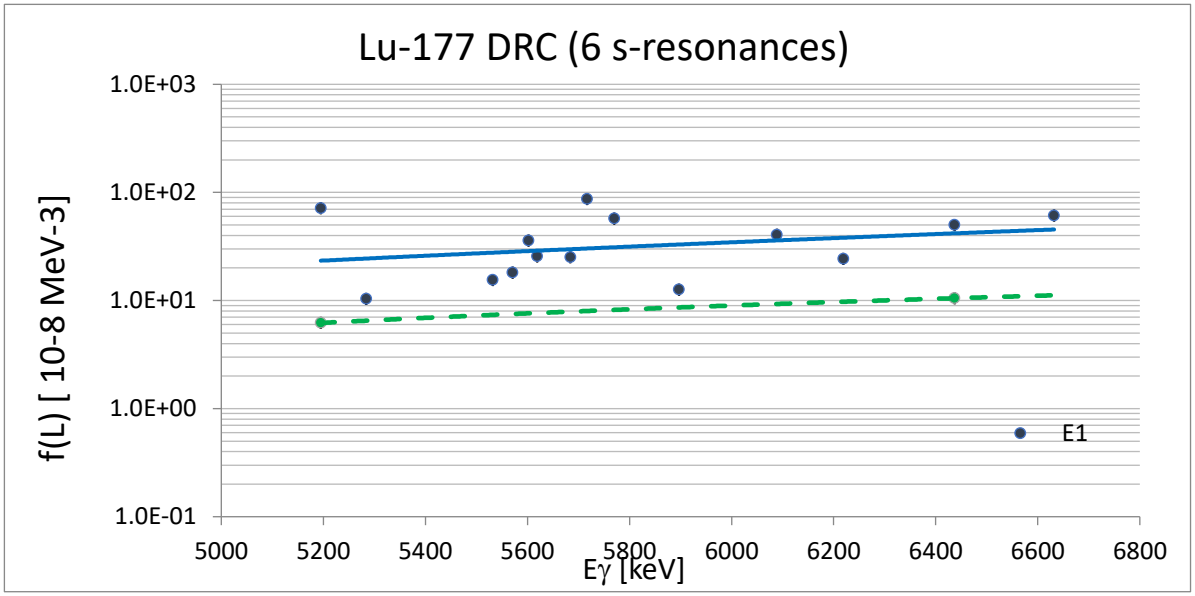

Th-233 DRC data BNL

Ig/1000 captures from T. von Egidy et al., Phys.Rev. C6 (1972) 266
5 s- resonances = J=1/2+ Gg = 0.0247 eV Do = 15.82 eV
Porter-Thomas dispersion estimate: 1+dPT =√2/υ=1.63
Statistical error assumed to be 25%

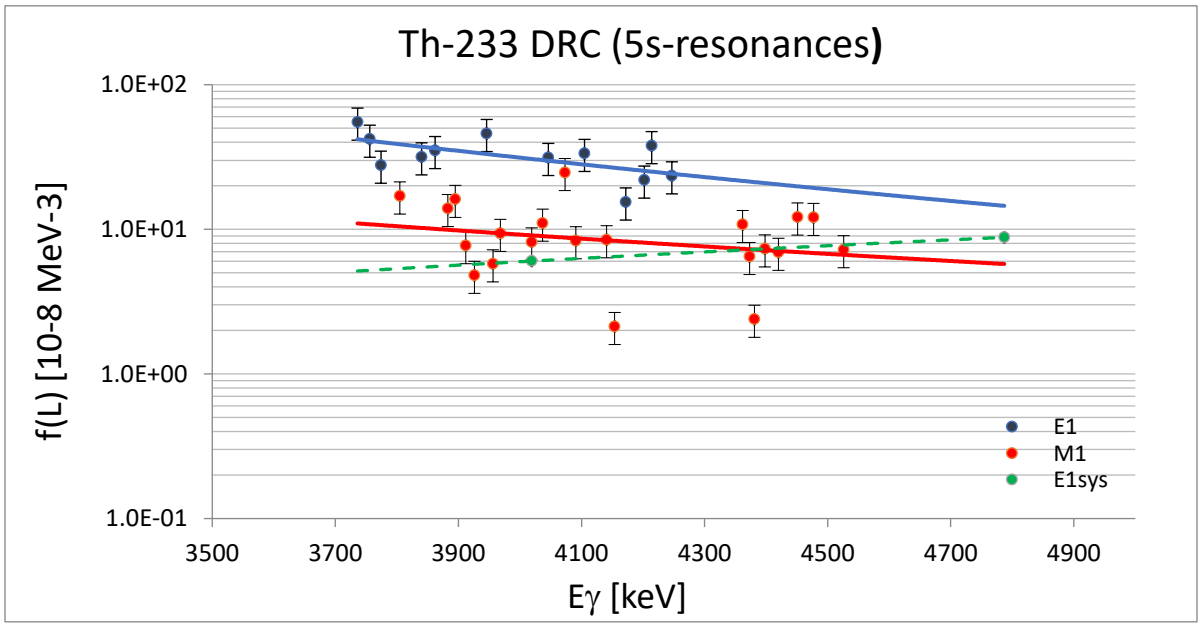

New evaluations

Ni-59 THC Mc Master

Ig/100 captures extracted from A.F.M. Ishaq et al. Zeit. Phys. A281 (1977) 365

Ggo = 2.03 eV Do = 12920 eV

Sum Ig = 101.0%

a = 1

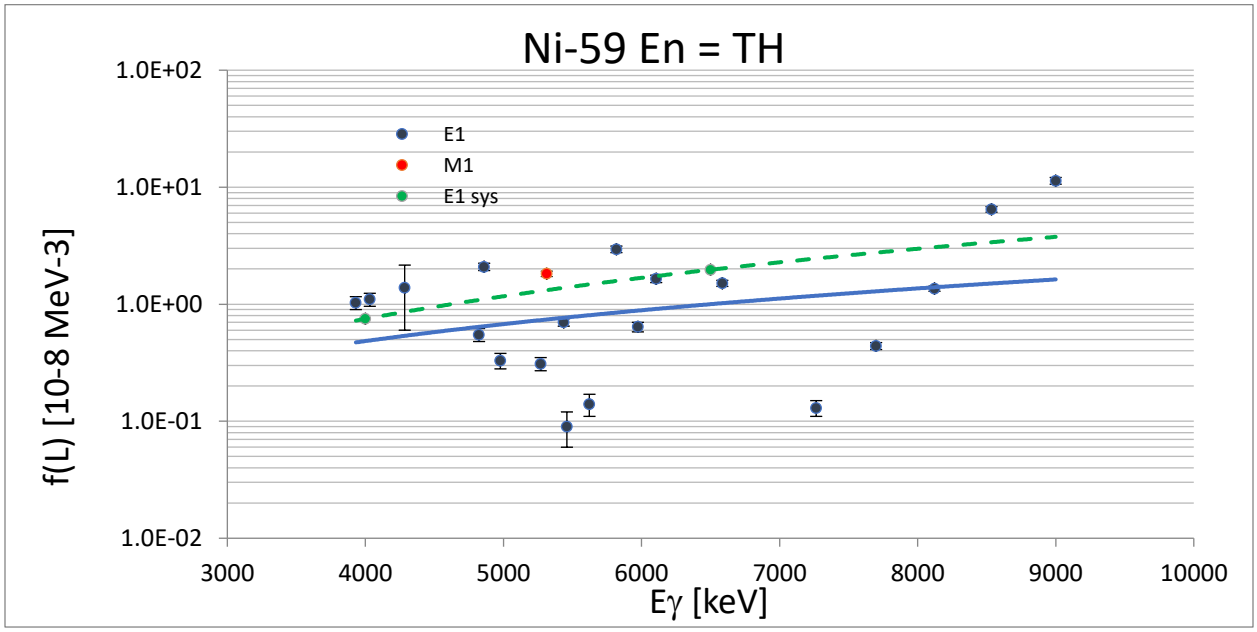

Ni-61 THC McMaster

Ig/100 captures extracted from A.F.M. Ishaq et al. Zeit. Phys. A281 (1977) 365

Ggo = 1.16 eV Do = 14500 eV

Sum Ig = 100.4%

a = 1

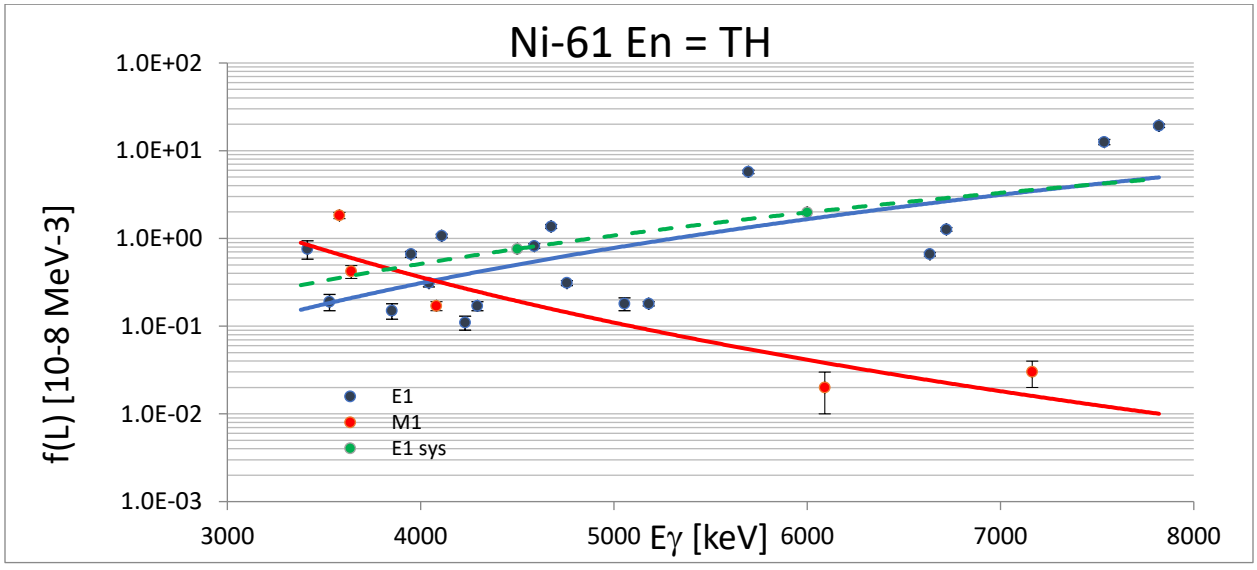

Ni-63 THC Mc Master

Ig/100 captures extracted from A.F.M. Ishaq et al. Zeit. Phys. A281 (1977) 365

Ggo = 0.91 eV Do = 16400 eV

Sum Ig = 101.7%

a = 1

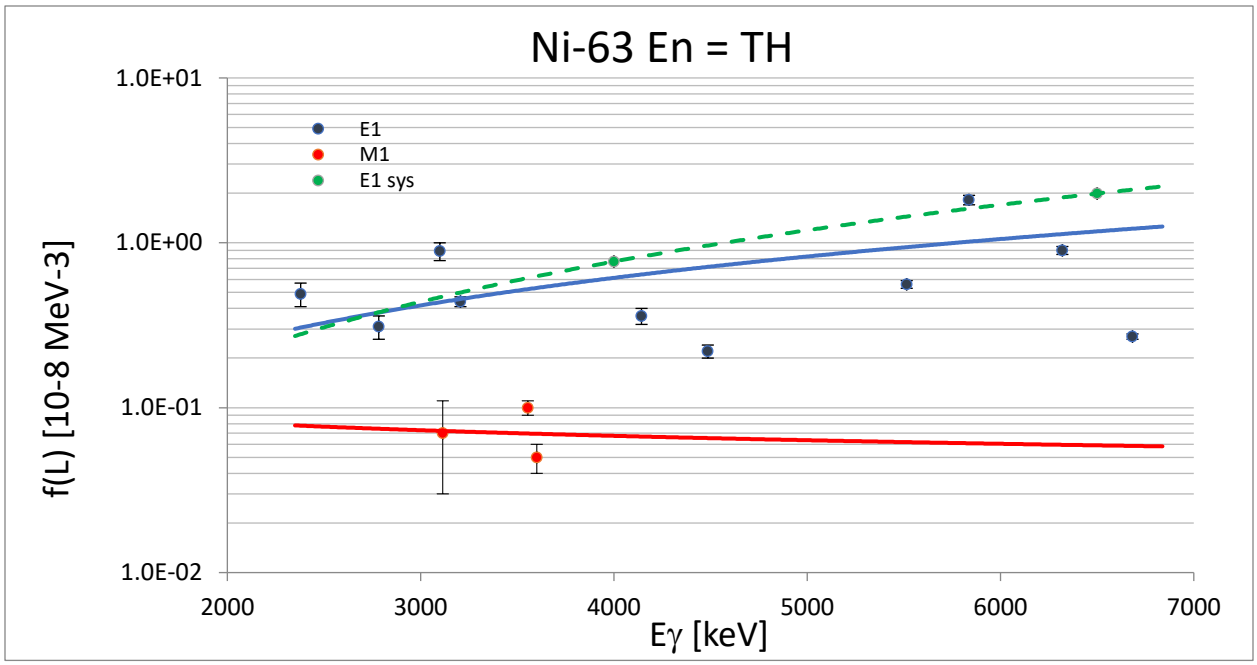

Zn-65 THC ECN-Jullich

Ig/100 captures extracted from J. de Boer et al. KFA-IKP-10/77 (1977) p.51

Ggo = 0.726 eV Do = 2940 eV

Sum Ig = 100.2%

a = 1

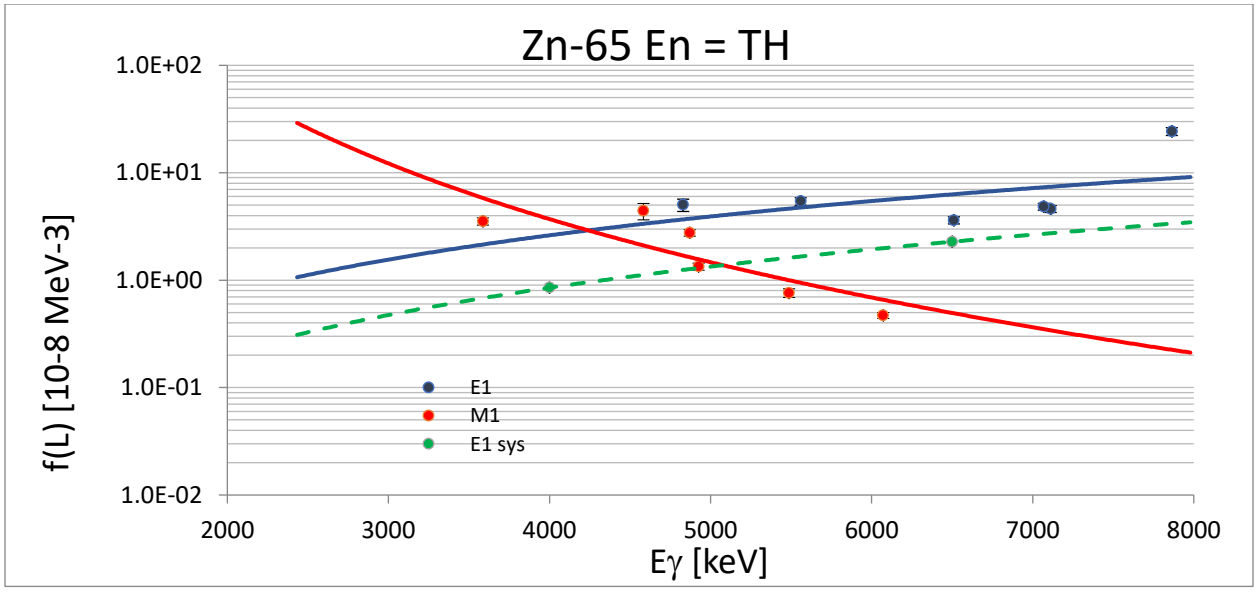

Zn-68 KfK

Ig/relative extracted from H. Ottmar et al. Nucl.Phys. A164 (1971) 69
normalized to 3 EGAF data <Eg> = 6.8 MeV f(E1) = 3.8(8) x-08MeV**3
Ggo = 0.44 eV Do = 367 eV
Sum Ig = 100.2%
a = 1

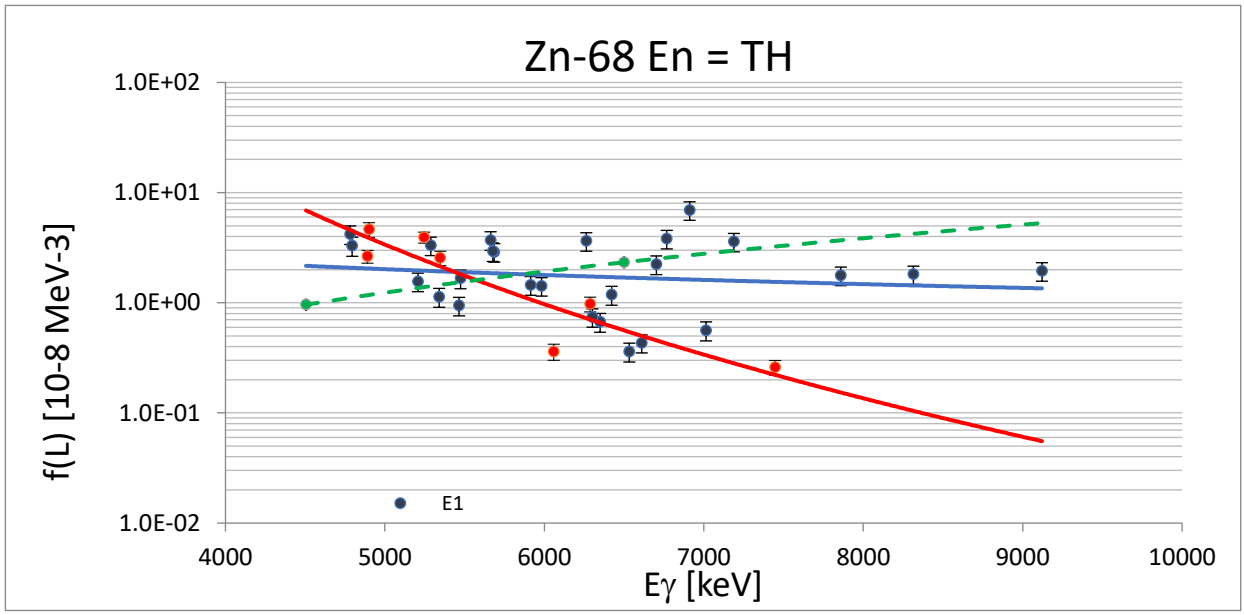

Nb-94 THC McMaster

Ig/10**5 captures extracted from T.J. Kennet et al., Ca. J. Phys. 66 (1988) 947
Do = 95.6 eV Ggo = 0.173 eV
Sum Ig = 125%
a = 0.52

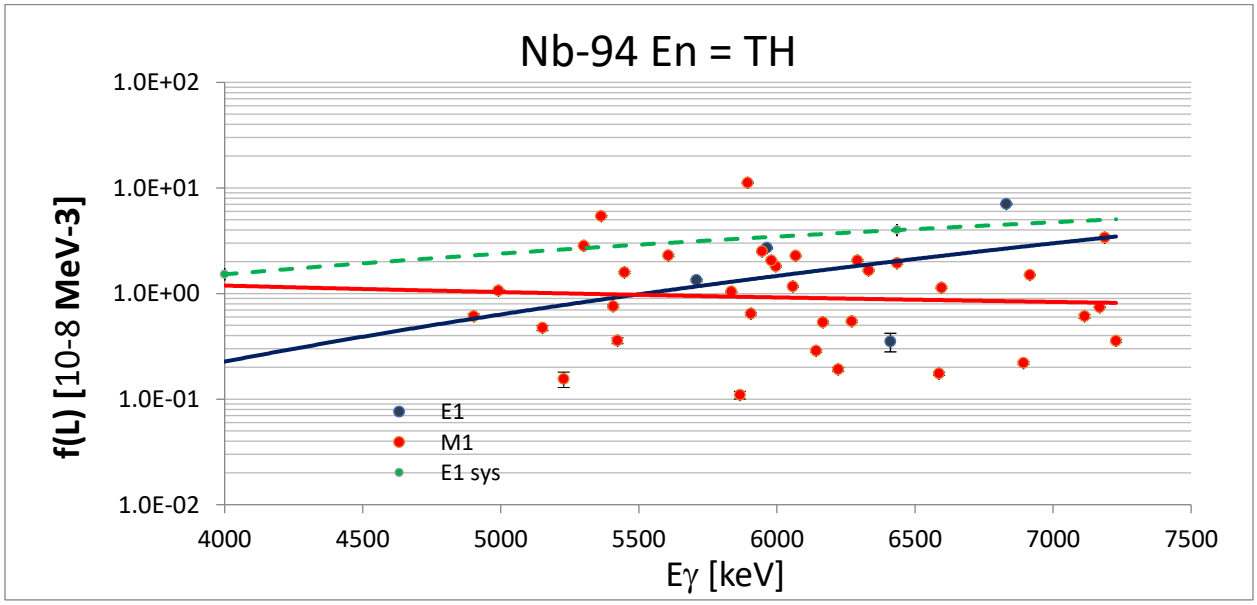

Ru-100 THC MacMaster

Ig/100 captures from M. Aslam et al., Can.J. Phys. 69 (1991) 658
100 captures corrected to 1000 captures based on <f(M1)> = 3.42(15) 10-8 from the paper
Ggo = 0.194 eV Do = 22 eV
Sum Ig = 120.4 adopted 89.9

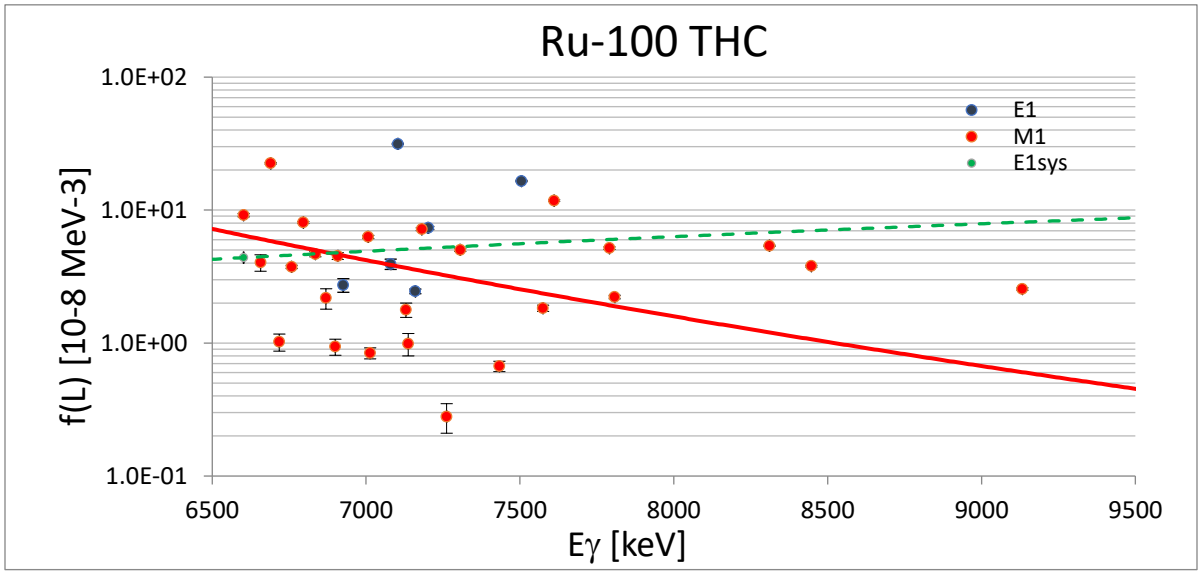

Ru-102 THC MacMaster

Ig/100 captures extracted from M. Aslam et al., Can.J. Phys. 69 (1991) 658
100 captures corrected to 1000 captures based on <f(M1)> = 8.2(41) 10-8 from the paper
Gg = 0.183 eV Do = 18.5 eV
Sum Ig = 129.2% adopted 84.5%
a = 0.73

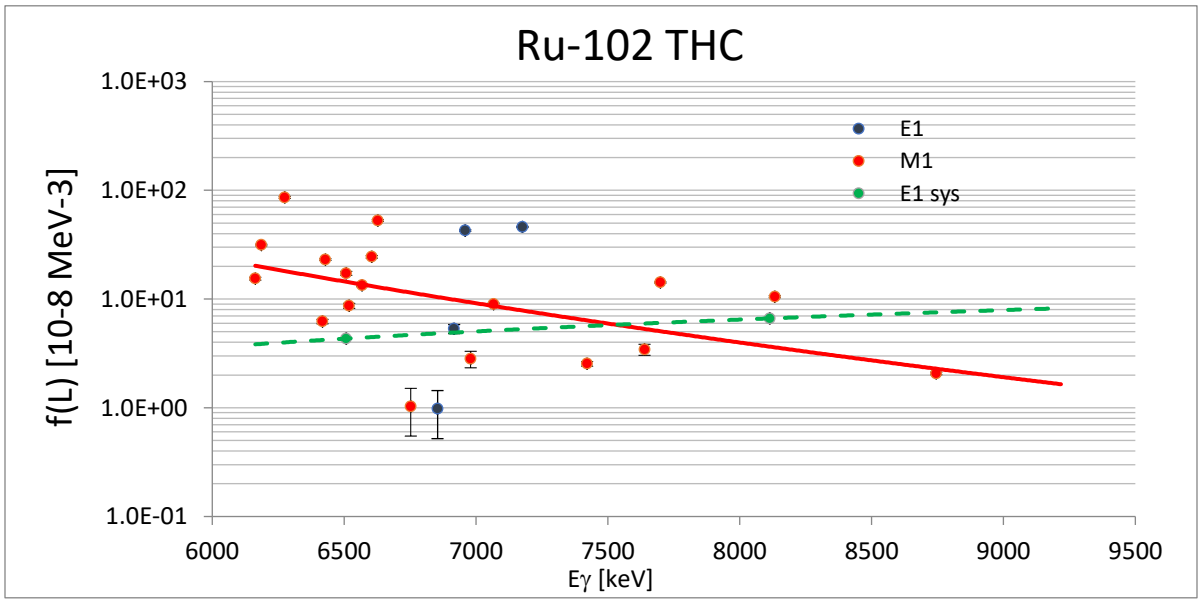

Yb-174 THC Idaho

Ig/100 captures extracted from R.C. Greenwood and C.W. Reich, Phys.Rev. C23 (1981) 153
Ggo = 0.074 eV Do = 8.06 eV
Sum Ig = 119%
a = 0.54

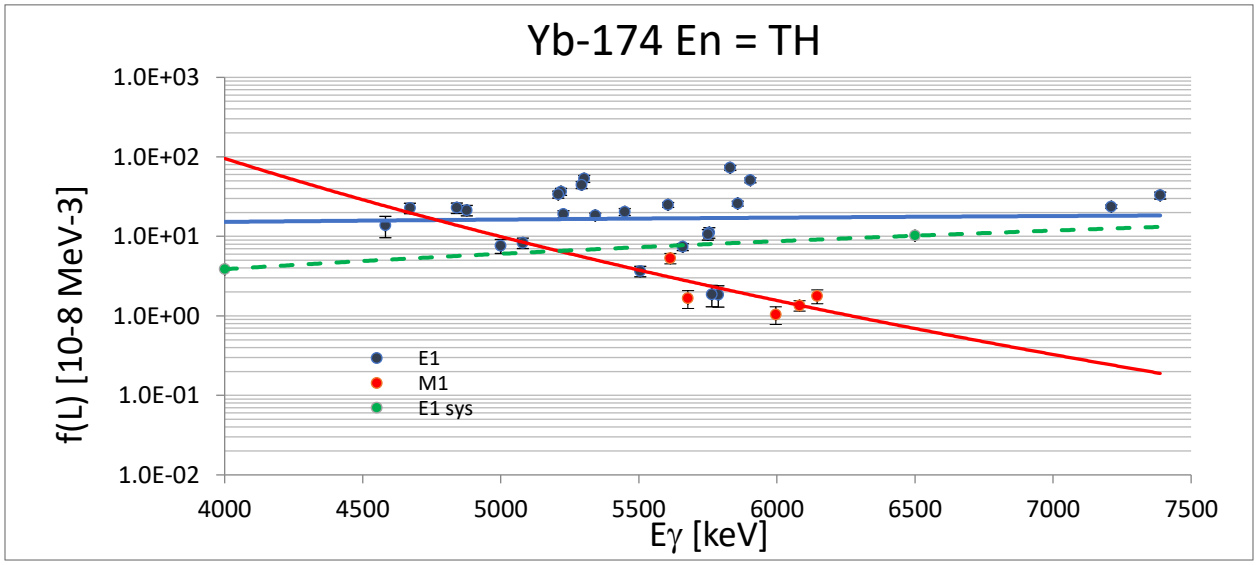

Lu-177 THC Los Alamos

Ig/1000 captures extracted from H.Minor et al., Phys.Rev. C3 (1971) 766
Ggo = 0.063 eV Do = 1.61 eV
Sum Ig = 66.9%
a = 0.01

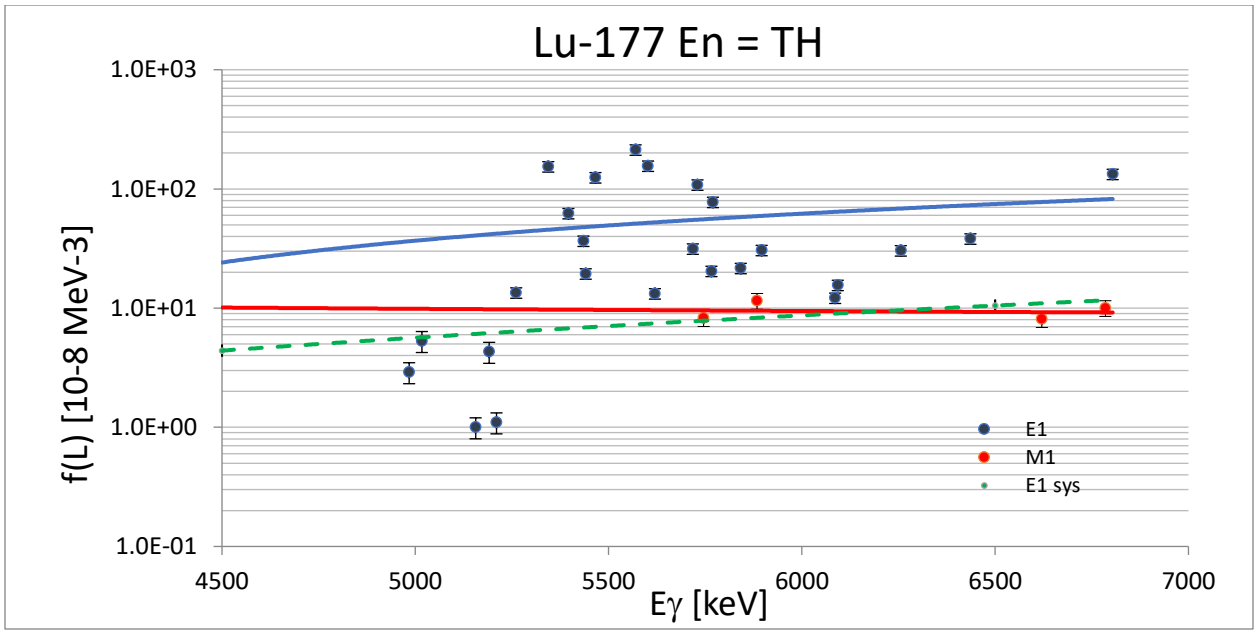

W-184 THC Idaho

Ig/100 captures extracted from R.C. Greenwood and C.W. Reich, Nucl.Phys. A223 (1974) 66
Ggo = 0.073 eV Do = 13.7 eV
Sum Ig = 25%
a = 0.86

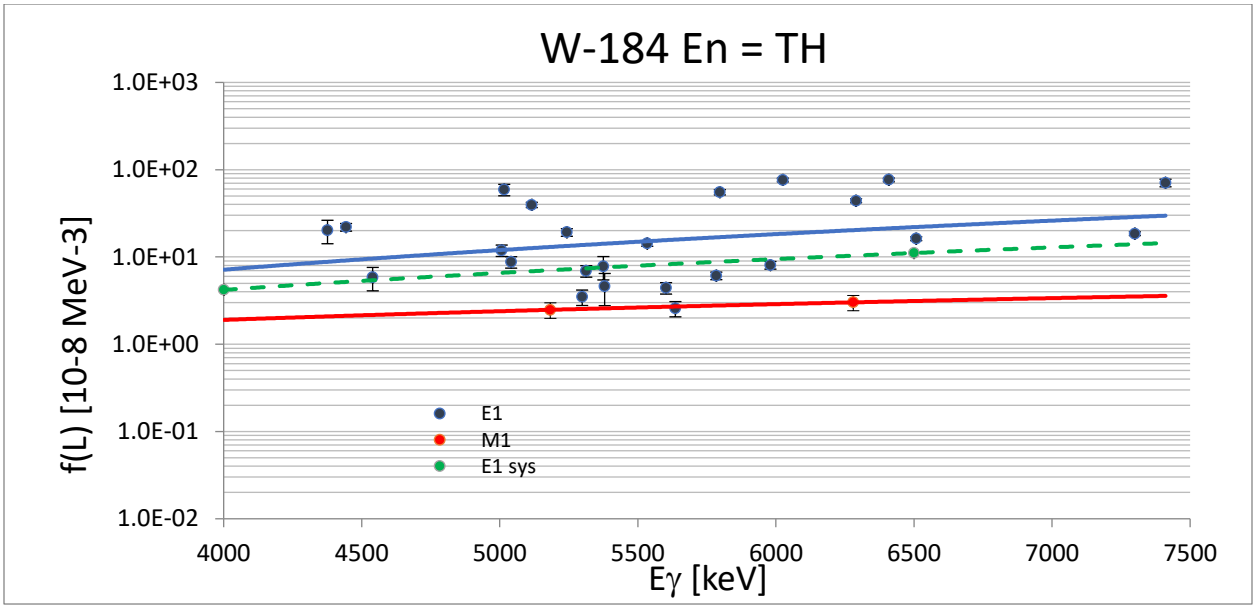

Th-233 THC Fribourg

Ig/1000 captures from J. Kern and D.Duc., Phys.Rev. C10 (1974) 1554
Ggo = 0.0247 eV Do = 15.82 eV
Sum Ig = 8.59
a = 1

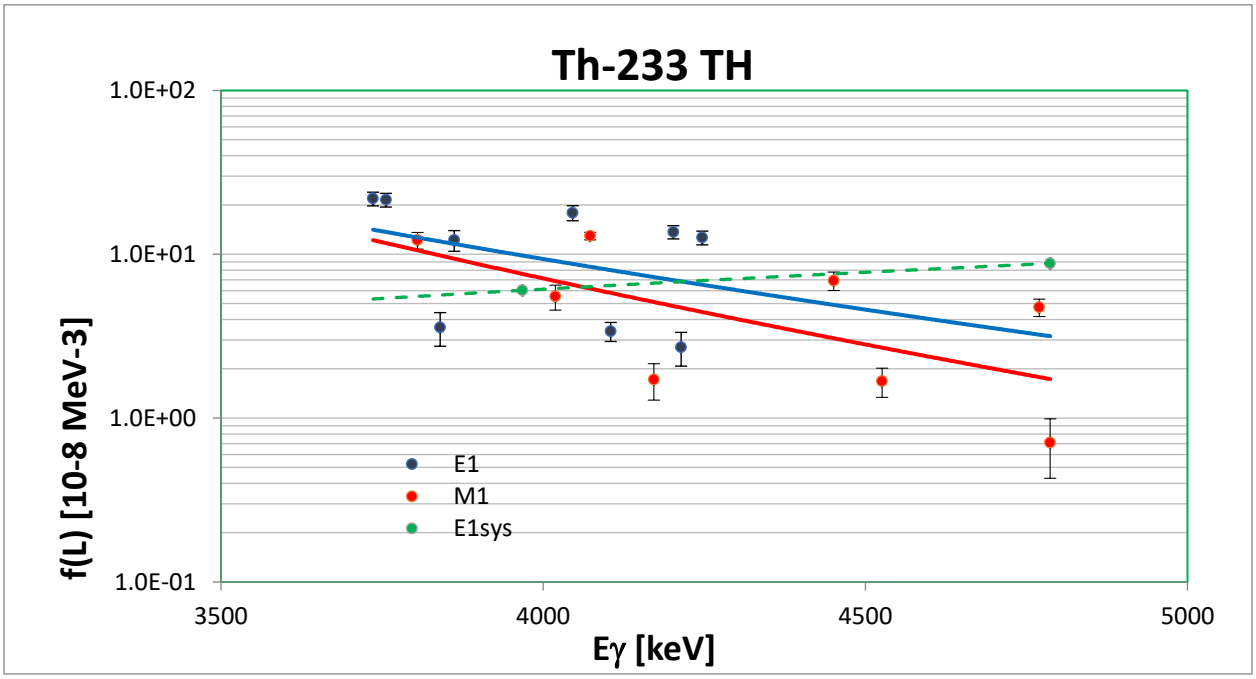

Nuclear Data Section
International Atomic Energy Agency
Vienna International Centre, P.O. Box 100
A-1400 Vienna, Austria

E-mail: nds.contact-point@iaea.org
Fax: (43-1) 26007
Telephone: (43-1) 2600 21725
Web: http://www-nds.iaea.org